RSC Advances

PAPER

View Article Online
View Journal | View Issue

Cite this: *RSC Adv.*, 2022, **12**, 22266

Light-emitting diode (LED)-directed green synthesis of silver nanoparticles and evaluation of their multifaceted clinical and biological activities

Sumaira Anjum, *[a] Rimsha Chaudhary,[a] Amna Komal Khan,[a] Mariam Hashim,[a] Iram Anjum,[a] Christophe Hano [b] and Bilal Haider Abbasi [c]

The trend of using plant extracts for the synthesis of nanoparticles has increased in recent years due to environmental safety, low cost, simplicity and sustainability of the green route. Moreover, the morphology of NPs can be fine-tuned by applying abiotic factors such as LEDs, which enhance the bio-reduction of the precursor salt and excite phytochemicals during their green synthesis. Considering this, in present study, the green synthesis of AgNPs was carried out using *Dalbergia sissoo* leaf extract under the illumination of red, green, blue, yellow and white LEDs. The phytochemical profile of the leaf extract in terms of total phenolic and flavonoid content was responsible for the effective synthesis of AgNPs, where alcohols and phenols were mainly involved in the capping and bio-reduction of the NPs. Moreover, the XRD data showed the face center cubic crystalline nature of the AgNPs with the interesting finding that the LEDs helped to reduce the size of the AgNPs significantly. Among the samples, Y-DS-AgNPs (34.63 nm) were the smallest in size, with the control having a size of 87.35 nm. The LEDs not only reduced the size of the AgNPs but also resulted in the synthesis of non-agglomerated AgNPs with different shapes including spherical, triangular, and hexagonal compared to the mixed-shape control AgNPs, as shown by the SEM analysis. These LED-directed AgNPs showed extraordinary therapeutic potential especially B-DS-AgNPs, which exhibited the highest anti-oxidant, anti-glycation and anti-bacterial activities. Alternatively, Y-DS-AgNPs were the most cytotoxic towards HepG2 cells, inducing intracellular ROS/RNS production, accompanied by a disruption in the mitochondrial membrane potential, caspase-3 gene activation and induction of caspase-3/7 activity. Lastly, AgNPs showed mild toxicity towards brine shrimp and moderately hemolyzed hRBCs, showing their biosafe nature. Here, we conclude that external factors such as LEDs are effective in controlling the morphology of AgNPs, which further enhanced their therapeutic efficacy.

Received 6th June 2022
Accepted 25th July 2022

DOI: 10.1039/d2ra03503k

rsc.li/rsc-advances

1. Introduction

There is an emerging trend of using greener approaches in every area of research to improve and protect the environment. Accordingly, a recent focus in the field of nano-biotechnology is the synthesis of nanoparticles (NPs) using biological entities, which overcomes the disadvantages of physicochemical methods for the synthesis of NPs. Amongst the various biological entities used for the green synthesis of NPs, plant-mediated synthesis has attracted the most attention given that it is a simple, rapid, energy efficient and eco-friendly method with easy handling and availability of plants throughout the year.[1]

Therefore, in our study, the green synthesis of silver nanoparticles (AgNPs) was carried out using *Dalbergia sissoo* leaf extract, which possesses a high level of phytochemicals such as iso-flavones, coumarins, neoflavonols and flavonols having biological properties including antimicrobial, analgesic, anti-oxidant, anti-inflammatory, antipyretic and osteogenic properties.[2] Many medicinally important plants have been explored by researchers for the synthesis of AgNPs; however, the synthesis of light-emitting diode (LED)-exposed AgNPs from *D. sissoo* has not been reported to date. The role of LEDs in the chemical/physical synthesis of AgNPs has been reported by many scientists but the plant-mediated synthesis of AgNPs under LED exposure has scarcely been studied. LEDs have high energy bands, small divergent angle and high emission intensity, and therefore they can be used as a source of excitation in photochemical reactions, which play a role in the size- and shape-controlled synthesis of NPs.[3]

Lee *et al.*[4] explored the role of sunlight and different LEDs on the *S. miltiorrhiza*-mediated synthesis of AgNPs. Their results

[a]*Department of Biotechnology, Kinnaird College for Women, 92-Jail Road, Lahore-54000, Pakistan. E-mail: sumaira.anjum@kinnaird.edu.pk; Tel: +92-3006957038*

[b]*Laboratoire de Biologie des Ligneux et des Grandes Cultures, INRAE USC1328, University of Orleans, 45067 Orléans CEDEX 2, France*

[c]*Department of Biotechnology, Quaid-i-Azam University, Islamabad-45320, Pakistan*

showed the generation of surface plasmon resonance (SPR) bands due to the excitation of free electrons in the AgNPs under LED illumination, resulting in their faster synthesis. The rationale for the use of LEDs for the effective synthesis of NPs includes their high photon efficiency, power stability, low voltage of electricity and low cost,[5] making them suitable for the large-scale synthesis of eco-friendly AgNPs.

Among the metallic nanoparticles, AgNPs are the most important due to their extensive biomedical applications, as evident by the fact that they are the most commercialized NPs with a production of about 500 tons per year.[6] AgNPs are considered to be safe and biocompatible given that a clinical study reported no clinically important toxic effects of commercial colloidal silver products on patients when administered as an antibacterial agent.[7] Recently, Wypij *et al.*[8] showed the anti-bacterial and anti-cancerous activities of biogenic AgNPs as an alternative treatment option. The other biomedical applications of AgNPs include their beneficial role in treating diabetes-related complications and aging through the inhibited formation of advanced glycation end-products (AGEs).[9] The significant therapeutic applications of AgNPs is accredited to their capability to scavenge reactive nitrogen species and reactive oxygen species, which is termed antioxidant activity. AgNPs mediate their antioxidant activity by neutralizing free radicals *via* hydrogen atom transfer or electron transfer.[10] The efficiency of NPs greatly depends on their morphological properties, which can be tuned by factors such as LED exposure during their synthesis. Therefore, this research work sheds light on the role of LEDs (green, blue, red, white and yellow) in fine-tuning the morphological characteristics of AgNPs synthesized *via* the green route, and subsequently their influence on the biological applications of AgNPs including anti-bacterial, anti-oxidant (FRAP, CUPRAC, ORAC and ABTS), anti-glycation, anti-cancer (cell viability, mitochondrial membrane potential, intracellular ROS/RNS generation, caspase-3 gene expression and caspase-3/7 activity), biocompatibility with hRBCs and toxicity against brine shrimp larvae.

2. Materials and methods

All chemicals used in this study were purchased from Sigma-Aldrich, USA, and used as received without further purification.

2.1. *Dalbergia sissoo* leaf extract preparation

Leaves of *D. sissoo* (sheesham) were freshly plucked and verified by the Department of Botany, Kinnaird College for Women, Lahore. 10 g leaves was dry weighed and washed with tap water and distilled water thrice. The washed leaves were set to boil in 400 mL distilled water on a burner and its volume reduced to 100 mL. The mixture was ground in a pestle and mortar and filtered with Whatman's filter paper. The leaf extract filtrate was stored at 4 °C for the synthesis of AgNPs.

2.2. Evaluation of phytochemical content and free radical scavenging activity of *Dalbergia sissoo* leaf extract

The total phenolic contents (TPC) of the *D. sissoo* leaf extract was measured by Folin–Ciocalteu's method, while the total flavonoid content (TFC) was measured using the aluminum chloride colorimetric method according to Khan *et al.*[1] For TPC, 1 mL leaf extract or gallic acid standard (97.5%, 50–1000 μg mL^{-1}), 0.5 mL Folin–Ciocalteu's reagent and 5 mL distilled water were added to a test-tube. The mixture was shaken well and incubated at room temperature (RT) for 5 min, and 1.5 mL of 20% sodium carbonate (99.5%) and distilled water were added to make the total volume of 5 mL. The mixture developed a deep blue color. Lastly, the mixture was incubated for 2 h at RT and the absorbance of the standard was measured at 750 nm using a spectrophotometer (Analytik Jena, Specord 200 plus, Jena, Germany). The TPC value of the leaf extract was measured from a gallic acid standard curve ($y = 0.00004x + 0.0089$, $R^2 = 0.9953$) and expressed as mg g^{-1} of gallic acid equivalent in milligrams per gram (mg_{GAE} g^{-1}) of dry extract.

For TFC, 1 mL *D. sissoo* extract/quercetin standard (25–200 μg mL^{-1}), 0.2 mL of 1 M potassium acetate (99.99%), 5.6 mL distilled water and 0.2 mL of 10% (w/v) $AlCl_3$ (98%) were added to a test tube, shaken and incubated for 30 min at RT. The absorbance of the standard was measured at 415 nm using a spectrophotometer. The TFC value of the leaf extract was measured from the standard curve of quercetin ($y = 0.0057x + 0.0127$, $R^2 = 0.9973$) and expressed as quercetin equivalent (QE) per gram DW.

TPC and TFC were measured using following equation:

$$\text{TPC/TFC} = \frac{C \times V\ (\text{mL})}{m\ (\text{g})} \quad (1)$$

Free radical scavenging activity (FRSA) was evaluated to measure the antioxidant potential of the *D. sissoo* leaf extract using DPPH (2,2-diphenyl-1-picrylhydrazyl, 97%) according to the protocol reported by Anjum *et al.*[11] Briefly, 0.5 mL leaf extract and 4.5 mL DPPH (3.2 mg/100 mL methanol) were mixed in a test tube and incubated for 1 h at RT. The absorbance of the mixture and standard was measured using a spectrophotometer at 517 nm. FRSA was expressed as a percentage of discoloration of DPPH calculated from the equation as follows:

$$\text{FRSA}\ (\%) = 100 \times \left(1 - \frac{\text{absorbance of plant extract}}{\text{absorbance of standard}}\right) \quad (2)$$

and the experiment was performed in triplicate.

2.3. Green synthesis of AgNPs under LED exposure

AgNPs were synthesized using the leaf extract under LED exposure, as reported by Anjum *et al.*[12] with minor modification. 0.01 M sliver nitrate solution (SNS, 99.99%) and 1 mL leaf extract (LE) were mixed in 12 v/v ratios (*i.e.*, 1 : 1, 1 : 2, 1 : 3, 1 : 4, 1 : 5, 1 : 6, 1 : 7, 1 : 8, 1 : 9, 1 : 10, 1 : 15 and 1 : 20) to identify an appropriate ratio for the optimal synthesis of AgNPs. Accordingly, 1 : 4 was selected as the best, given that an instant color change from greenish yellow to dark brown was observed and it showed stability without a change in absorbance even after 1 month. Using a ratio of 1 : 4, AgNPs were synthesized under exposure to 5 types of LEDs including red (640–650 nm), blue (460–465 nm), green (530–540 nm), white (450–455 nm) and yellow (590–595 nm). All the LEDs had a luminous intensity of 17 000 mcd, with the typical voltage of 3.1–3.4 V and forward

current of 20 mA. For the preparation of AgNPs, the mixture of SNS and LE was continuously stirred under exposure to each LED together with constant monitoring using a UV-Visible spectrophotometer. After the synthesis of the AgNPs using each LED, the reaction mixture was micro-centrifuged at 13 000*g* rpm for 10 min, and then the pellets were re-suspended in distilled water. This step was repeated thrice. The control *D. sissoo*-mediated AgNPs (DS-AgNPs) and five different types of AgNPs were formed, *i.e.*, red LED mediated (R-DS-AgNPs), blue LED mediated (B-DS-AgNPs), green LED mediated (G-DS-AgNPs), white LED mediated (W-DS-AgNPs) and yellow LED mediated (Y-DS-AgNPs), which were subjected to further characterization and biological activities.

2.4. Characterization of LED-mediated green-synthesized AgNPs

The AgNPs were characterized using techniques including UV-Visible spectroscopy, scanning electron microscopy (SEM), energy-dispersive X-ray (EDX), Fourier-transform infrared spectroscopy (FTIR) and X-ray diffraction (XRD).

The progress of the green synthesis of AgNPs under LED illumination was checked by recording their UV–Vis spectra in the range of 350–750 nm using a spectrophotometer.

The FTIR analysis was performed following the method reported by Tungmunnithum *et al.*[13] using a Bruker (Palaiseau, France) V70 interferometer in the wavenumber range of 400–4500 cm^{-1}.

The shape of the AgNPs was determined by SEM at different magnifications using a SIGMA model SEM (MIRA3; TESCAN, Brno, Czech Republic), while an EDX detector attached to the SEM was used to analyze the elemental composition and purity of the AgNPs.

The crystalline nature of the AgNPs was evaluated by XRD using an X-ray diffractometer (Shimadzu-Model, XRD6000). Furthermore, the size of the AgNPs was calculated using the Debye–Scherrer equation.[14]

2.5. Antibacterial activities of LED-mediated green-synthesized AgNPs

The antibacterial activity of the AgNPs was evaluated against *Bacillus subtilis*, *Pseudomonas fluorescens* and *Pseudomonas aeruginosa* by the well-diffusion method, as described by Abbasi *et al.*[15] Firstly, stock cultures of *B. subtilis*, *P. aeruginosa* and *P. fluorescens* were revived on nutrient agar (NA) followed by swabbing a single colony of the bacterial strains on Mueller-Hinton agar (MHA) to assess the antibacterial activity of the AgNPs. 15 μL of 0.1 M SNS (positive control), LE (negative control), 10 mg mL^{-1} AgNPs and 10 μg per disc tetracycline antibiotic discs (Thermo Fisher Scientific™ Oxoid™) were added to the wells on MHA plates. The plates were incubated at 37 °C overnight and the zones of inhibition were measured in millimeters (mm).

2.6. Antioxidant activities of LED-mediated green-synthesized AgNPs

2.6.1 Ferric reducing antioxidant power assay (FRAP). The FRAP assay was adopted from Abbasi *et al.*,[16] where 10 μL of AgNPs was mixed with 190 μL of FRAP solution (20 mM of 97% grade $FeCl_3$, 300 mM acetate buffer (pH 3.6), 10 mM TPTZ of 98% purity and 6 mL H_2O v/v). The reaction mixture was incubated at RT for 15 min and the absorbance was measured using a BioTek ELX800 absorbance microplate reader at 630 nm.

2.6.2 Cupric reducing antioxidant capacity (CUPRAC). The CUPRAC assay was performed as reported by Karaman *et al.*[17] with slight changes. For this study, a mixture of 1 mL copper chloride (99.99%), 1 mL neocuproine solution and 1 mL of 1 M acetate buffer (pH 7) was prepared. 1 mL distilled water was added to 1 mL of AgNPs and incubated at RT for 30 min and the absorbance at 450 nm measured. To this mixture, the cupric reaction mixture was added and incubated for another 30 min at 50 °C in test tubes. These test tubes were then cooled under running tap water and maintained at RT followed by measurement of their absorbance at 450 nm against the blank. The standard calibrations of each AgNPs (control, red, blue, green, white and yellow) were plotted as the absorbance (*x*-axis) *vs.* molar concentration (*y*-axis) and the molar absorptivity of AgNPs was measured from the calibration curve.

2.6.3 2(2,2-Azinobis-3-ethylbenzthiazoline-6-sulphonic acid) assay (ABTS). The ABTS assay was replicated as reported by Thaipong *et al.*[18] with slight changes. Stock solutions of 7.4 mM ABTS (98%) and 2.6 mM potassium persulfate (99.99%) were prepared and mixed in equal quantities to make a standard solution. This standard solution was incubated at RT for 12 h in the dark and diluted by adding 1 mL ABTS with 60 mL methanol followed by measuring its absorbance at 734 nm. This ABTS solution was then mixed with each type of AgNPs (control, red, blue, green, white and yellow LED) and incubated for 2 h in the dark. The absorbance was measured at 734 nm and compared with the standard curve. The results are expressed in μM Trolox equivalent antioxidant capacity.

2.6.4 Oxygen radical absorbance capacity (ORAC). The ORAC assay was adopted from the study by Abbasi *et al.*[16] Briefly, 190 μL of fluorescence reaction mixture in 75 mM phosphate buffer at pH 7.4 was added to 10 μL of AgNP solution and incubated at RT for 20 min on an orbital shaker. Then 20 μL of 119.4 mM 2,2′-azobisamidinopropane (97.5%) was added to the fluorescence mixture and its intensity measured at 5 min intervals for 2.5 h at room temperature using a fluorescence spectrophotometer (Bio-Rad) with the absorbance set at 485 nm and emission wavelength at 535 nm.

2.7. Anti-glycation activities of LED-mediated green-synthesized AgNPs

The anti-glycation activity of the AgNPs was measured as % inhibition of AGEs by following the protocol of Shah *et al.*[19] The AgNP solution was mixed with 20 mg mL^{-1} BSA solution (Sigma Aldrich) prepared in phosphate buffer (0.1 M; pH 7.4), 1 mL of phosphate buffer (0.1 M; pH 7.4) containing sodium azide 0.02% (w/v) and glucose solution (0.5 M; Sigma Aldrich) prepared in phosphate buffer and incubated for 5 days at 37 °C in the dark. The formation of the fluorescent AGEs was verified using a VersaFluor fluorometer (Bio-Rad, France) with the emission and excitation wavelengths set at 410 nm and 330 nm, respectively.

2.8. Anti-cancerous activities of AgNPs

2.8.1 Measurement of cell viability of HepG2 cells. The cell viability of human liver cancer cells (HepG2) (ATCC HB-8065; American Type Culture Collection, USA) was measured using the MTT (3-(4,5-dimethylthiazolyl-2)-2,5-diphenyltetrazolium bromide) dye to evaluate the cytotoxicity of the AgNPs *in vitro*. HepG2 cells were cultured in Dulbecco's modified Eagle's medium. 200 μg mL^{-1} of AgNPs was added to a 96-well plate pre-seeded with HepG2 cells (>90% viability; 1×10^4 cells per well; 200 μL per well), for 24 h. Then 10 μL MTT dye (5 mg mL^{-1}) was added per well and incubated for 3 h. The insoluble formazan was dissolved with 10% acidified sodium dodecyl sulfate. After overnight incubation of the cells, the absorbance of the plates was measured at 570 nm using a microplate reader (Platos R, 496. AMP, AMEDA Labordiagnostik GmbH, Graz, Austria). All the experiments were performed in triplicate. Non-treated cells (NTC) were used as the control. Cell viability is expressed as percentage and measured using the following equation:

$$\text{Viability } (\%) = \frac{\text{Sample absorbance} - \text{control absorbance}}{\text{NTC absorbance} - \text{media absorbance}} \times 100 \quad (3)$$

2.8.2 Evaluation of intracellular reactive oxygen and nitrogen species (ROS/RNS) production. Intracellular ROS/RNS production was measured by following the method by Nazir *et al.*[20] Pre-seeded HepG2 cells in a 96-well plate were washed with phosphate-buffer saline (PBS) twice and suspended in PBS having 0.4 μM fluorescent dihydrorhodamine-123. The mixture was incubated in the dark for 10 min at 30 °C and its fluorescence measured (λ_{em} = 535 nm, λ_{ex} = 505 nm) using a Versa-Fluor Fluorimeter (Biorad, France).

2.8.3 Mitochondrial membrane potential (MMP) measurement. The MMP of HepG2 cells treated with the AgNPs was measured using 3,3′-dihexyloxacarbocyanine iodide ($DiOC_{6(3)}$, 98%), as described previously by Khan *et al.*[1] HepG2 cells were incubated in culture medium containing 25 nM $DiOC_{6(3)}$ for 40 min at 37 °C. MMP is expressed as relative fluorescent units (RFU).

2.8.4 Caspase-3 gene expression and caspase-3/7 activity. To measure the expression of the caspase-3 gene, firstly the isolation of total RNA was carried out using the GeneJET RNA Purification Kit (Thermo Scientific) followed by quantification using the Quant-iT RNA Assay Kit (Invitrogen). The reverse transcription of RNA was carried out using the First-strand cDNA Synthesis Kit (Thermo). PikoReal quantitative PCR was performed using the DyNAmoColorFlash SYBR Green qPCR Kit (ThermoFisher). The caspase-3 primers included 5′-CACGCCATGTCATCATCAAC-3′ (reverse primer) and 5′-TGTTTGTGTGCTTCTGAGCC-3′ (forward primer) (amplicon size: 210 bp). The data was analyzed using the Pikoreal software.

The Apo-ONE Homogeneous Caspase-3/7 Assay kit (Promega) was used to evaluate *in vitro* caspase-3/7 activity following the manufacturer's instructions. All the data was measured in triplicate.

2.9. Biocompatibility of AgNPs

2.9.1 Lethality of AgNPs against brine shrimp. The lethality of the AgNPs was measured against *Artemia salina* (brine shrimp) in a 96-well plate (300 μL) for 24 h, as described by Ahmed *et al.*[21] Firstly, eggs of *A. salina* were hatched by incubating them for 24–48 h in a plastic tray containing 38 g L^{-1} sterile sea water supplemented with dried yeast (6 mg L^{-1}) and a suitable oxygen supply. Ten mature nauplii (phototropic) were taken and AgNPs (25, 50, 100, and 200 μg mL^{-1}) were added to the well and the final volume was made up to 300 μL. 1% DMSO (99.99%) in sea water was used as the negative control and doxorubicin as the positive control. Lethal concentration (LC_{50}) was measured by using the table curve 2D v5.01 of AgNPs with ≥50% mortality.

2.9.2 Biocompatibility with human red blood cells (hRBCs). The hemo-compatibility of the AgNPs with RBCs was measured by using blood samples from one female and 2 males (average age 28 years) after obtaining consent. The blood samples were collected in EDTA vacutainers, which prevented blood clotting. This experiment was carried out in accordance with the ethical standards of the International and National Research Committees as well as the 1964 Helsinki Declaration and its later amendments due to the involvement of human participants.[22] After extracting RBCs, erythrocytes and 100 μL AgNPs were taken in an Eppendorf tube, which was incubated at 35 °C for 1 h and centrifuged at 10 000 rpm for 10 min. 100 μL supernatant was taken in a 96-well plate and a BioTek ELX800 absorbance microplate reader (BioTek Instruments, France) was used to measure the release of hemoglobin at 540 nm. Triton X-100 (positive) and DMSO (negative) acted as the controls. The results are expressed as % hemolysis using the following formula:

$$\text{Hemolysis } (\%) = \frac{\text{Sample absorbance} - \text{negative control absorbance}}{\text{Positive control absorbance} - \text{Negative control absorbance}} \times 100 \quad (4)$$

2.10. Statistical analysis

All data was evaluated statistically to measure the mean and standard deviation by using SPSS (Windows Version 7.5.1, SPSS Inc., Chicago, IL, USA). The data was expressed as mean ± SD.

3. Results and discussion

3.1. Evaluation of phytochemical content and free radical scavenging activity of *Dalbergia sissoo* leaf extract

The leaf extract of *D. sissoo* was rich in phenolic content, where in our study the TPC was measured to be 23.6 ± 0.76 mg_{GAE} g^{-1} DW. In accordance with our findings, Kamboj *et al.*[23] also reported a high TPC of 31.29 ± 0.29 mg GA/100 g in *D. sissoo*. The enriched phenolic content indicates the good metal chelating and reducing potential of *D. sissoo* leaf extract during the synthesis of NPs.

The TFC of *D. sissoo* calculated for this study was 1.65 ± 0.01 mg_{QE} g_{DW}^{-1}. Yasmeen *et al.*[24] reported the highest TFC in an

aqueous leaf extract of *D. sissoo* (156.66 ± 0.002 $mg_{QE}\ g_{extract}^{-1}$) compared to the bark and fruit aqueous extract. In numerous studies, flavonoids are reported to be the major contributors during the plant-mediated synthesis of AgNPs given that hydroxyl groups play a role in reducing Ag ions into AgNPs.[25]

The FRSA of the *D. sissoo* leaf extract was found to be 80.84% ± 0.87%. Previous studies have also shown the significant antioxidant activities of *D. sissoo* extract such as 13.19% FRSA at 300 μg mL^{-1} concentration was reported for its methanolic extract.[26] Our findings suggest that aqueous *D. sissoo* extracts have significant antioxidant potential, which means effective metal ion reduction during the biosynthesis of NPs by electron donation.

3.2. Optimization of green synthesis of AgNPs

For the synthesis of AgNPs, firstly the v/v ratio of leaf extract (LE) and silver nitrate solution (SNS) was optimized (1 : 1, 1 : 2, 1 : 3, 1 : 4, 1 : 5, 1 : 6, 1 : 7, 1 : 8, 1 : 9, 1 : 10, 1 : 15 and 1 : 20) and the best ratio showing the fastest synthesis and stabilization was chosen. Among the ratios, 1 : 1, 1 : 2 and 1 : 20 did not show any peak when monitored using a Specord-200 UV-Vis spectrometer in the wavelength range of 350–750 nm. In contrast, 1 : 4 was selected as best given that its synthesis and capping were completed within 24 h without a change in absorbance (Fig. 1). The intensity of the color change increased with time to a darker tone. All ratios were observed at room temperature for 6–48 h. After 24 h of reaction, no increase in color change and absorbance was observed in the 1 : 4 ratio, whereas in the case of the 1 : 5, 1 : 6 and 1 : 7 reaction mixtures, there was no change in color but the absorbances of all these ratios kept changing even after 48 h of incubation, which indicated the instability of the AgNPs synthesized using these ratios. Among the ratios tested, the reaction mixture of 1 : 4 showed no change in absorbance after 24 h, which indicates the high stability of the AgNPs synthesized in this ratio. Moreover, the highest absorbance was also shown by the 1 : 4 reaction mixture among the ratios, which indicates the highest yield of AgNPs. Due to the higher stability and yield of the 1 : 4 reaction mixture, this ratio was selected for the further synthesis of AgNPs under different LED illumination.

The synthesis and stabilization of all the AgNPs in all ratios were monitored between 6–48 h, as shown in Fig. 2a and b. Initially, no peaks were observed for the 1 : 1, 1 : 7, 1 : 9 and 1 : 20 ratios after 6 h of incubation, indicating no AgNPs were synthesized using these ratios. Even the 1 : 20 ratio showed no peak after 24 h of incubation, where the synthesis started in this ratio after 48 h of incubation. In contrast, there was an increase in the absorbance of the 1 : 4 ratio between 6–24 h but no change after 24 h, which indicates that the synthesis of AgNPs was completed without a further increase in absorbance after 48 h of incubation (Fig. 2c). Alternatively, with an increase in reaction time, the other ratios show distorted peaks or no significant increase in absorbance, which suggests the slow and unstable synthesis of AgNPs. It was found that the 1 : 4 ratio showed the highest absorbance (4.23) with a stable peak among the tested ratios. Jalab *et al.*[27] evaluated the effect of the optimum extract and sliver nitrate ratio and concluded that an

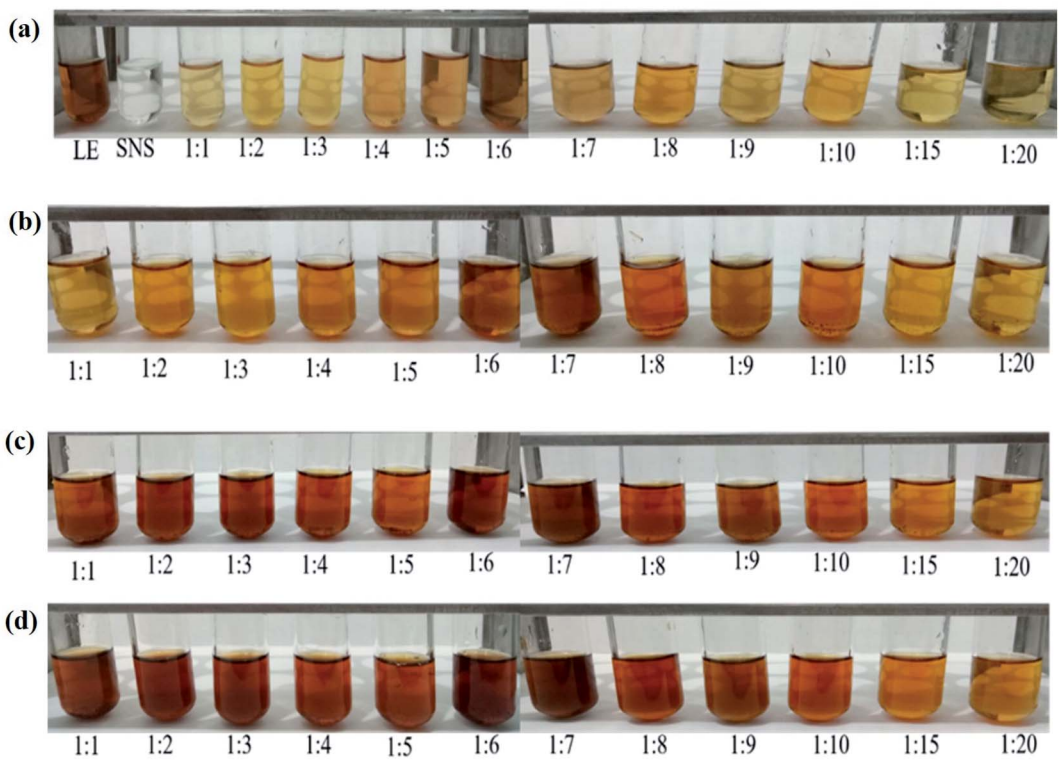

Fig. 1 Optimization of AgNPs at different ratios (v/v LE/SNS). (a) Initial change in color of reaction mixtures (LE + SNS) in all ratios. (b) Change in color of reaction mixture after 6 h incubation. (c) Change in color after 24 h incubation. (d) Color change after 48 h incubation.

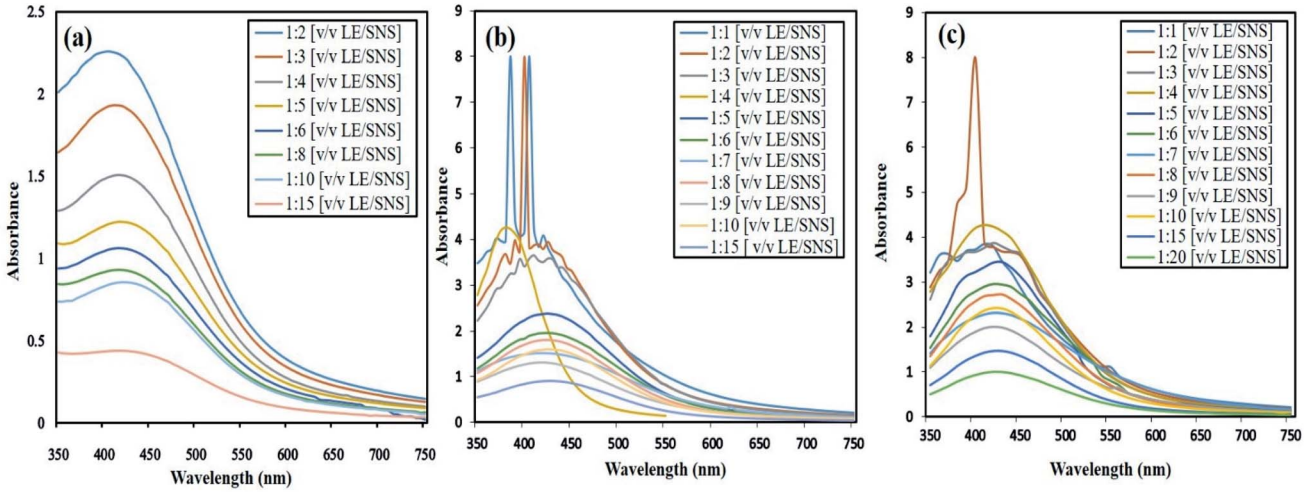

Fig. 2 Optimization of 12 ratios of AgNPs. (a) UV-visible spectra at 6 h, (b) 24 h and (c) 48 h incubation period.

increase in the extract concentration yielded bigger-sized AgNPs.

3.3. Characterization of LED-mediated green-synthesized AgNPs

3.3.1 UV-visible spectroscopy. UV-Vis spectroscopy was employed to evaluate the synthesis and stabilization of the LED-mediated green-synthesized AgNPs in aqueous solution. Using a 1 : 4 ratio of LE and SNS, AgNPs were synthesized under LED exposure, and as shown in Fig. 3a–d, after 30 min of blue and red LED exposure, distorted peaks were formed between 420–440 nm. Meanwhile, the AgNPs synthesized with exposure to green, yellow and white LEDs were stable for 2 h. Therefore, the green synthesis of AgNPs under each LED exposure was carried out for 30 min, given that distorted peaks were observed after 30 min. Nguyen *et al.*[28] also reported the accelerated bio-reduction of Ag ions under LED exposure, particularly a blue LED compared to the control. The UV-visible spectrum revealed the important role of SNS and phytochemicals in the synthesis of AgNPs. Peaks were observed between 400–450 nm for all the AgNPs, corresponding to the absorbance by AgNPs due to excitation of surface plasmon vibration.[29]

3.3.2 Fourier-transform infrared spectroscopy (FTIR). FTIR spectroscopy is useful for the identification of different

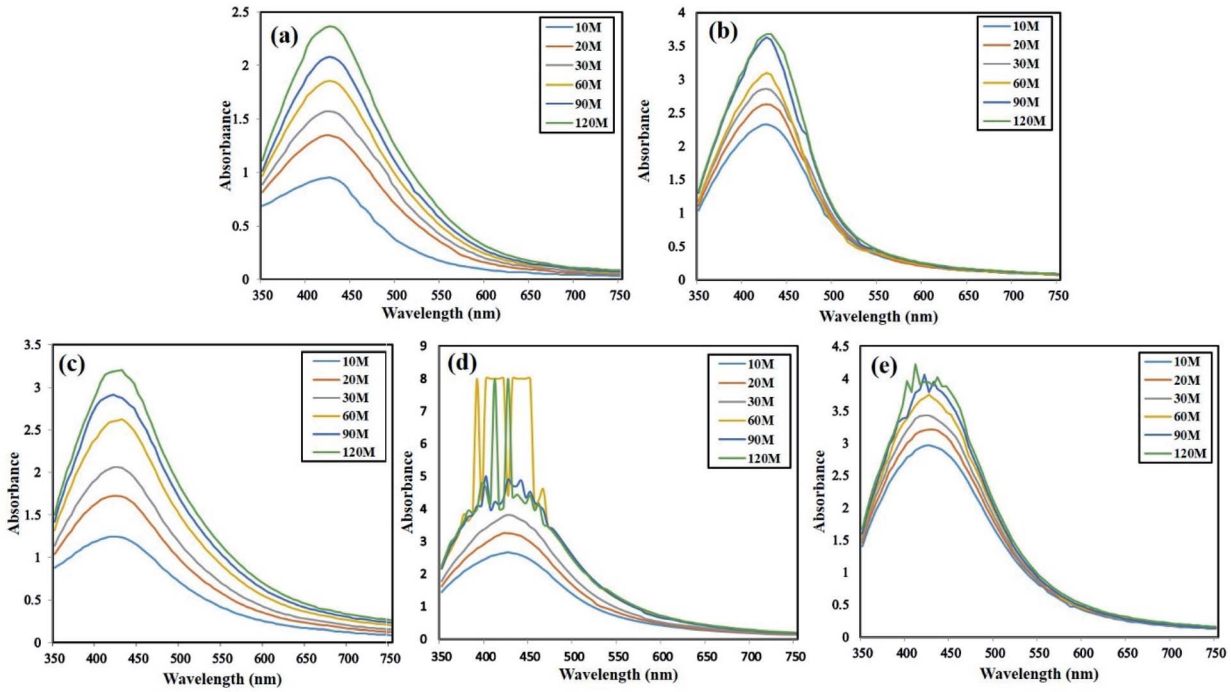

Fig. 3 UV-Visible spectra of (a) G-DS-AgNPs, (b) W-DS-AgNPs, (c) Y-DS-AgNPs, (d) B-DS-AgNPs and (e) R-DS-AgNPs.

functional groups present in active plant ingredients. Interpretation of the infrared absorption spectrum corresponds with the chemical bonds present in plant extracts.[30] The leaf extract of *D. sissoo* showed distinct peaks at 1263.23 cm^{-1}, 1643.16 cm^{-1}, 2069.38 cm^{-1}, 2360.60 cm^{-1} and 3367.32 cm^{-1} (Fig. 4a). These peaks correspond to the C–N stretch (aromatic amines), C=O– stretch (carbonyl group), –C≡C– stretch (alkynes), C=N stretch (nitriles) and N–H (1°, 2° amines, amides), respectively. Previous FTIR analysis of *D. sissoo* extract also showed the presence of alkenes (1613.62 cm^{-1}).[31] Fig. 4b–g show the FTIR spectra of the control and LED-mediated AgNPs. The results show a sharp peak at ~1643.16 cm^{-1}, which reflects the capping and stabilization of AgNPs by the carbonyl group C=O, as also reported by Bawazeer *et al.*[32] A broader peak at the frequency of 3500–3200 cm^{-1} is also observed in all types of AgNPs, which possibly means involvement of the O–H stretch, H–bonded phenols and alcohols in the bioreduction, capping and stabilization. Similarly, Varadavenkatesan *et al.* reported the presence of amides (3475.15 cm^{-1}), carboxyl (2925.23 cm^{-1}), amino groups (2364.12 cm^{-1}), polyphenols (1745.34 cm^{-1}) and secondary alcohols (1625.67 cm^{-1}) in green AgNPs synthesized from *Thunbergia grandiflora* flower extract.[33]

3.3.3 Scanning electron microscopy analysis. Scanning electron microscopy was carried out to determine the shapes of the AgNPs. Fig. 5a shows that the control DS-AgNPs (*D. sissoo*-mediated) were irregularly spherical in shape. In contrast, Fig. 5b and c show that G-DS-AgNPs and W-DS-AgNPs are distinctly spherical in shape, which can be ascribed to the lower energy of the LEDs. Moreover, the high-energy blue LED promoted the formation of non-spherical hexagonal-shaped AgNPs, which is similar to the report by Lee *et al.*[4] in which hexagonal-shaped *Salvia miltiorrhiza*-mediated AgNPs under a blue LED were formed. Moreover, irregular triangular-like-shaped Y-DS-AgNPs and R-DS-AgNPs were formed (Fig. 5d–f). In this study, LED exposure helped to re-define the morphology of the AgNPs, particularly the high-energy blue LED

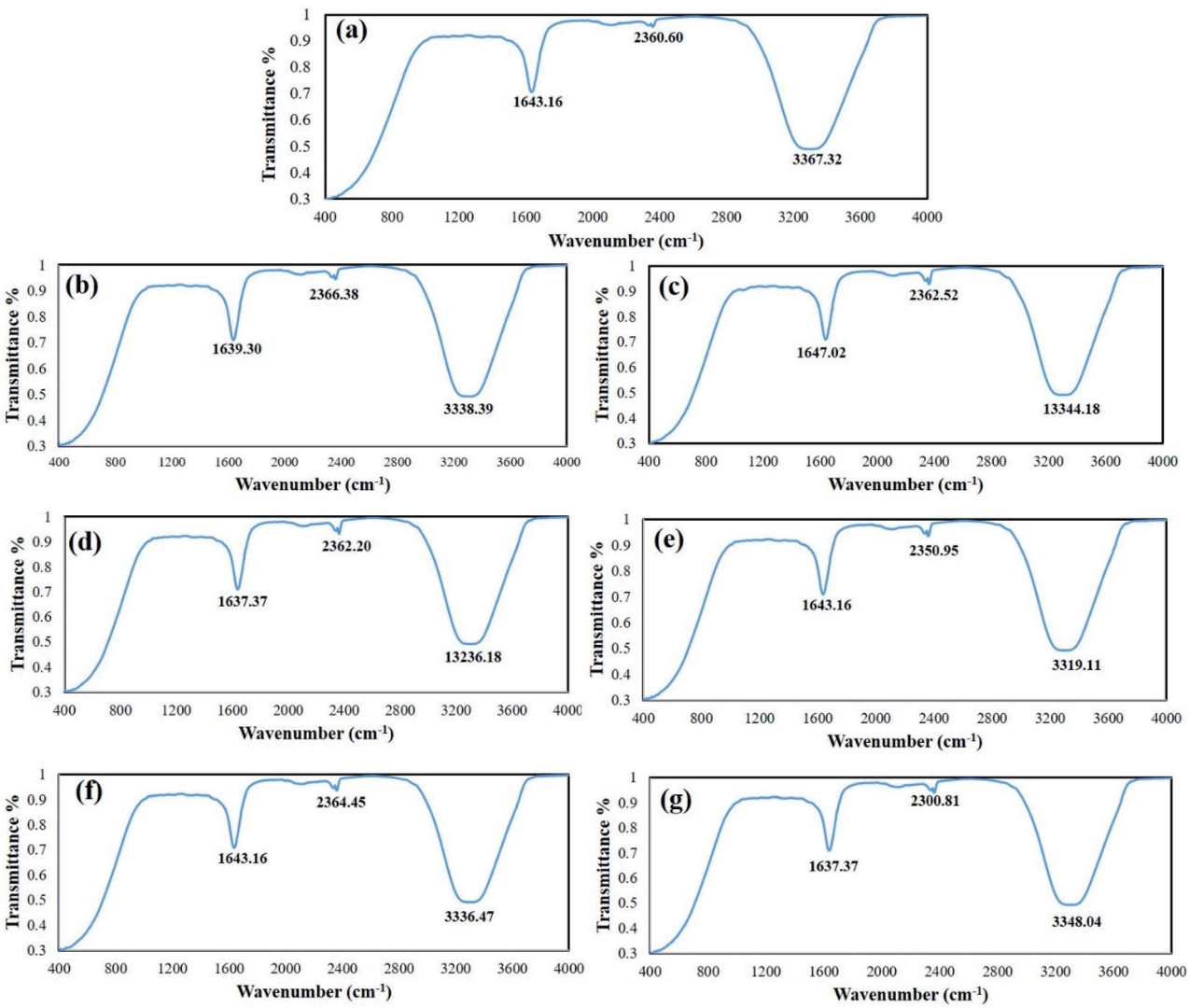

Fig. 4 FTIR analysis of (a) *D. sissoo* leaf extract, (b) DS-AgNPs, (c) G-DS-AgNPs, (d) W-DS-AgNPs, (e) Y-DS-AgNPs, (f) B-DS-AgNPs and (g) R-DS-AgNPs.

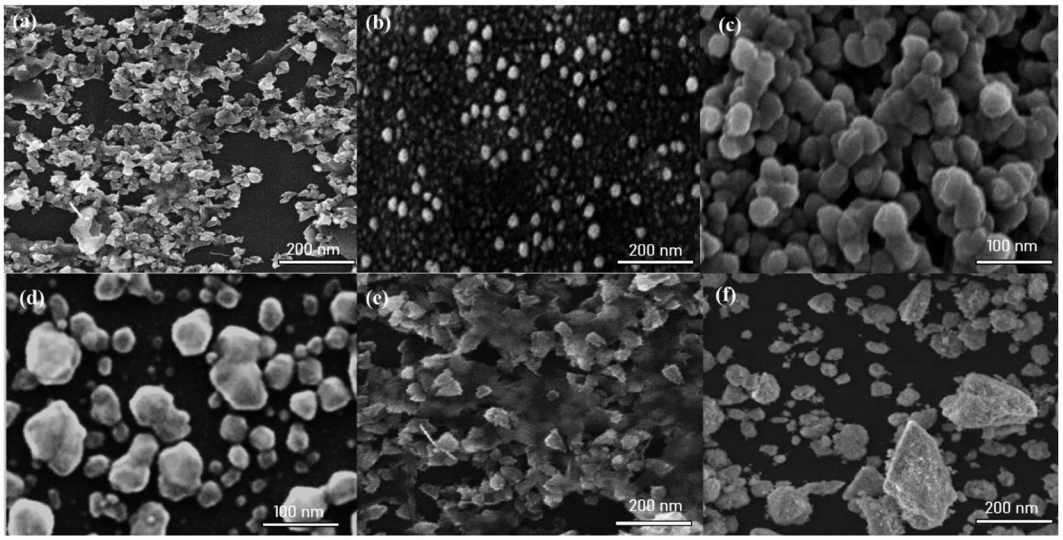

Fig. 5 SEM images of (a) DS-AgNPs, (b) G-DS-AgNPs, (c) W-DS-AgNPs, (d) B-DS-AgNPs, (e) Y-DS-AgNPs and (f) R-DS-AgNPs.

transformed the shape of the AgNPs into a non-spherical form. Moreover, LED exposure resulted in the formation of separate mono-dispersed AgNPs, which can be due to the capping of individual AgNPs by the phytochemicals present in the plant leaf extract, thus preventing their agglomeration. The LED lights helped to form distinct morphologies of AgNPs, which ultimately influence the efficacy of the NPs during biological applications.

3.3.4 Energy dispersive X-ray analysis. The elemental constituents, purity and relative abundance of the AgNPs were assessed by EDX. The strong signals between 2.5–4 keV were observed in all types of AgNPs (Fig. 6a–f), which is characteristic for the absorption of AgNPs and is consistent with previous reports.[34] The elemental percentage revealed 45.2% Ag in DS-AgNPs, while an increased elemental composition was observed in the AgNPs synthesized under LED illumination including G-DS-AgNPs (54.76%), R-DS-AgNPs (28.34%), Y-DS-AgNPs (68.54%), W-DS-AgNPs (63.24%) and B-DS-AgNPs (69.54%). These findings show the role of LEDs, particularly blue LED, in the effective biosynthesis of AgNPs. The Cu signal

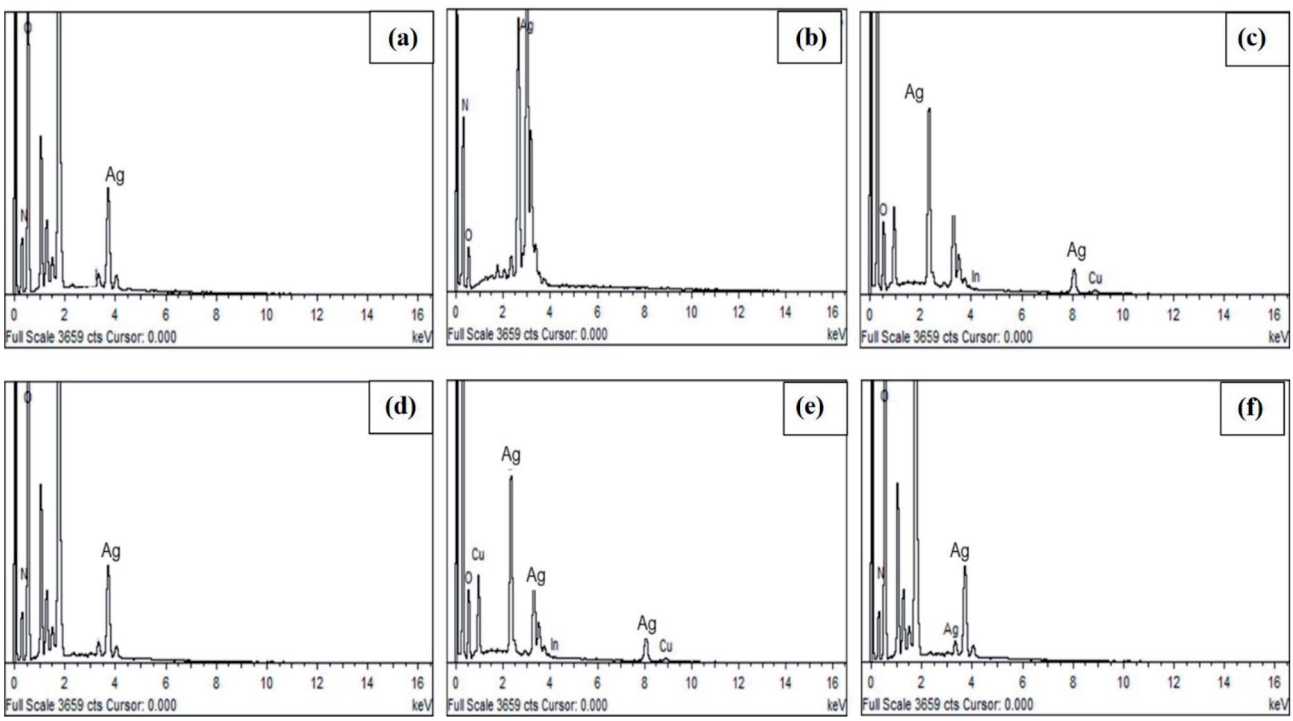

Fig. 6 EDX spectrum of (a) DS-AgNPs, (b) G-DS-AgNPs, (c) W-DS-AgNPs, (d) B-DS-AgNPs, (e) Y-DS-AgNPs and (f) R-DS-AgNPs.

was also observed in W-DS-AgNPs and Y-DS-AgNPs, which may have originated from the carbon-supported copper grid used for sample preparation.[35] The absence of other elements confirmed that the AgNPs were of high purity. Rautela *et al.*[36] also observed the high purity of AgNPs synthesized from *Tectona grandis* seed extract by EDX analysis.

3.3.5 X-ray diffraction analysis. XRD confirmed the crystalline structure and size of the AgNPs. Fig. 7a–f show the diffraction peaks of the AgNPs synthesized from *D. sissoo* under the influence of LEDs. Sharp and distinct peaks were observed at 2θ values of around 36°–38° (111), 44°–45° (200), 65°–66° (220) and 77°–78° (331) for all the AgNPs. These peaks confirm the face centered cubic (FCC) crystalline nature of the AgNPs, which is in agreement with the standard JCPDS card no. 04-0783. Soliman *et al.* also described the FCC crystallinity of the biosynthesized AgNPs at similar observed peaks.[37] Furthermore, the size of the AgNPs was calculated using Debye–Scherrer the equation, as summarized in Table 1. The sizes of the AgNPs are as follows: control DS-AgNPs (87.35 nm), W-DS-AgNPs (68.72 nm), R-DS-AgNPs (57.78 nm), G-DS-AgNPs (45.23 nm), B-DS-AgNPs (42.78 nm) and Y-DS-AgNPs (34.63 nm). These findings show a reduction in the size of AgNPs with a decrease in wavelength with the exception of Y-DS-AgNPs. Furthermore, a marked difference in the size of the control AgNPs and AgNPs synthesized under LED illumination was observed, which suggests the role of LEDs in exciting electrons and phytochemicals during the synthesis of AgNPs, hence fine-tuning their size. Similarly a reduction in size, *i.e.*, 18.5 nm (white), 28.02 nm (green), 50.22 nm (red), 16.26 nm (blue) and 10.12 nm (sunlight) and formation of unique-shaped AgNPs was observed with a decrease in the wavelength of the different types of LEDs in a previous report.[4] Similarly, a reduction in the size of AgNPs was observed when the light source was changed from white (40–100 nm) to blue LED (20–80 nm) during the capulin cherry-mediated synthesis of AgNPs.[5]

Table 1 The average diameter of AgNPs in nm calculated using XRD data

Type of AgNPs	Average diameter (nm)
DS-AgNPs	87.35
G-DS-AgNPs	45.23
W-DS-AgNPs	68.72
B-DS-AgNPs	42.78
Y-DS-AgNPs	34.63
R-DS-AgNPs	57.78

3.4. Antibacterial activities of LED-mediated green-synthesized AgNPs

Nano-sized AgNPs display significant antibacterial activity over a wide spectrum of bacterial species. Interestingly, AgNPs are reported as safe for use in humans, and therefore they are permitted to be used as antibacterial nanomedicines. The antibacterial activity of the LED-mediated green-synthesized AgNPs was evaluated against *Bacillus subtilis*, *Pseudomonas aeruginosa* and *Pseudomonas fluorescens*. These bacterial strains are reported to cause various diseases in plants, animals and humans. *Bacillus subtilis* was reported to cause various infections such as bacteremia, endocarditis, pneumonia, and septicemia and also spoiled preserved foods.[38] *Pseudomonas aeruginosa* is a Gram-negative bacteria and has also been reported to cause infections in the blood, lungs (pneumonia), and other parts of the body after surgery.[39] Similarly, *Pseudomonas fluorescens* is a rod-shaped Gram-negative bacterium species, reported to cause infections in humans (bacteremia) and animals including otitis and urinary tract infections in dogs, mastitis in dairy cows and endometritis in horses.[40] To avoid these infections, AgNPs proved to be the best candidates due to their excellent antibacterial activities.[41–43]

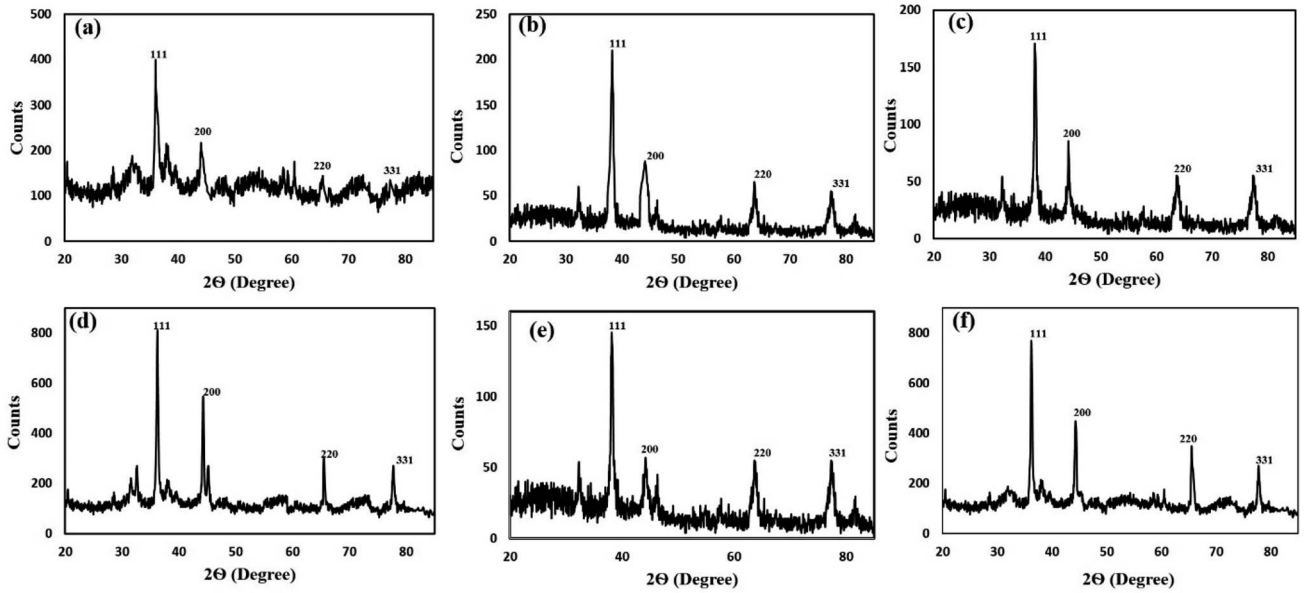

Fig. 7 X-ray diffractogram of (a) DS-AgNPs, (b) G-DS-AgNPs, (c) W-DS-AgNPs, (d) B-DS-AgNPs, (e) Y-DS-AgNPs and (f) R-DS-AgNPs.

Table 2 Zone of inhibition formed by AgNPs measured against different bacteria

Bacterial strain	Sample type	Mean of zone of inhibition (mm) (15 μL per well)					
		DS-AgNPs	G-DS-AgNPs	W-DS-AgNPs	B-DS-AgNPs	Y-DS-AgNPs	R-DS-AgNPs
Bacillus subtilis	Negative control (LE)	5 ± 0.96	4.5 ± 0.23	4 ± 1.54	4.5 ± 1.22	5 ± 1.2	4 ± 0.88
	Positive control (SNS)	10 ± 1.2	10 ± 1.91	9 ± 1.77	10 ± 2.08	10 ± 2.1	9 ± 1.86
	AgNPs	11 ± 1.5	11 ± 1.74	7 ± 1.09	11 ± 2.13	8 ± 1.14	7 ± 1.42
	Standard test disc	13 ± 1.7	14 ± 2.64	14 ± 2.41	14 ± 2.93	12 ± 2.82	14 ± 2.92
Pseudomonas aeruginosa	Negative control (LE)	5 ± 0.7	5 ± 0.92	5 ± 0.9	5 ± 0.94	5.5 ± 1.19	6.5 ± 1.23
	Positive control (SNS)	6 ± 1.07	7.5 ± 1.33	6.5 ± 1.1	8 ± 1.27	6.5 ± 1.4	7 ± 1.6
	AgNPs	5.5 ± 0.6	7.5 ± 1.64	7 ± 1.54	8 ± 1.25	8 ± 1.87	7 ± 1.15
	Standard test disc	10 ± 0.99	9.5 ± 1.79	8.5 ± 1.73	10.5 ± 1.5	9 ± 1.78	6.5 ± 1.23
P. fluorescence	Negative control (LE)	5 ± 0.31	5 ± 0.38	5 ± 1.07	5 ± 0.99	5 ± 1.2	5 ± 0.99
	Positive control (SNS)	6.5 ± 0.64	6 ± 1.28	6.5 ± 1.20	6.5 ± 1.1	6 ± 1.56	6 ± 1.23
	AgNPs	7.5 ± 1.62	7.5 ± 1.55	8 ± 1.41	9.5 ± 1.3	8.5 ± 1.66	8 ± 1.62
	Standard test disc	7 ± 1.33	7 ± 1.42	7.5 ± 1.09	6 ± 1.2	7.5 ± 1.88	7.5 ± 1.52

To evaluate the antibacterial activities of the LED-mediated AgNPs, the leaf extract of *D. sissoo* was used as a negative control, while SNS as a positive control. Our research showed that all the AgNPs showed considerable antibacterial activity, where a prominently higher zone of inhibition was formed against the Gram-positive *B. subtilis* compared to the Gram-negative *Pseudomonas* strains (Table 2). Fig. 8a–f show that B-DS-AgNPs and G-DS-AgNPs formed the highest zone of inhibition, *i.e.*, 11 mm against *B. subtilis*, followed by Y-DS-AgNPs (8 mm), while R-DS-AgNPs and W-DS-AgNPs formed 7 mm. These zones of inhibitions are still higher than that formed against the Gram-negative bacteria, which is in accordance with the conclusion by Ju *et al.*[44] that smaller-sized AgNPs formed an 11.4 mm zone of inhibition against the Gram-positive *B. subtilis*. Dutta *et al.*[45] also reported the strong anti-bacterial activity of green AgNPs against *B. subtilis*.

Fig. 8g–l show that B-DS-AgNPs and Y-DS-AgNPs formed the highest zone of inhibition (8 mm) against *P. aeruginosa*, which is a Gram-negative opportunistic pathogen. G-DS-AgNPs formed 7.5 mm, W-DS-AgNPs and R-DS-AgNPs formed 7 mm, while the control AgNPs formed a 5.5 mm zone of inhibition. A bio-informatic analysis found that the AgNPs mediated their anti-bacterial activity against *P. aeruginosa* by interfering with the cell membrane function and intracellular ROS generation.[46] Our results show that B-DS-AgNPs and Y-DS-AgNPs are efficient in inhibiting the growth of *P. aeruginosa*, which can be attributed to their smaller size and morphology.

P. fluorescens is another Gram-negative bacterium, which is known to contaminate packaged food.[47] In this study, we also tested the potential of the LED-mediated green-synthesized AgNPs to be used an antibacterial agent in food packaging. Fig. 8m–r show that B-DS-AgNPs formed a significant zone of inhibition of 9.5 mm, while G-DS-AgNPs formed least a 7.5 mm zone. In contrast, Y-DS-AgNPs, W-DS-AgNPs and R-DS-AgNPs formed intermediate zones of 8.5 and 8 mm. Daniel *et al.*[48] also reported the antibacterial activity of AgNPs synthesized from *Eichornia crassipes* against *P. fluorescens*, forming a 15 mm zone of inhibition.

3.5. Antioxidant activities of LED-mediated green-synthesized AgNPs

3.5.1 FRAP assay. FRAP is a robust, inexpensive and simple electron transfer (ET) method, which measures the ferric reducing ability of a test sample.[49] In this assay, the antioxidant potential of AgNPs was measured from the reduction of a ferric ion (Fe^{3+})–ligand complex into an intense blue color ferrous (Fe^{2+})–ligand complex in an acidic environment.[50] Commonly, tripyridyltriazine (TPTZ) is employed as the iron binding ligand, while Trolox as the positive control, and therefore the results are expressed as μM TEAC (Trolox equivalent antioxidant capacity).[51] In our study, the highest FRAP value of 485.6 ± 9.6 μM TEAC was recorded for B-DS-AgNPs, while Y-DS-AgNPs showed the lowest FRAP of 212.2 ± 10.8 μM TEAC (Fig. 9a). For R-DS-AgNPs, their FRAP was 431.1 ± 17.0 μM TEAC, G-DS-AgNPs 274.0 ± 15.4 μM TEAC, and W-DS-AgNPs 409.0 ± 7.1 μM TEAC, while control showed 369.9 ± 13.6 μM TEAC. Recently the antioxidant potential of green AgNPs measured in terms of FRAP was reported by Balciunaitiene *et al.*[52] Another study reported the antioxidant potential of AgNPs measured *via* the FRAP assay to be the highest of 176.91 μM TEAC.[19] Herein, our AgNPs showed even higher ferric reducing ability. The results show the significant antioxidant potential of AgNPs, particularly B-DS-AgNPs, which can be attributed to their fine-tuned morphology.

3.5.2 CUPRAC assay. The CUPRAC assay is a variant of the FRAP method, which uses copper as the oxidant in place of iron. In this assay, the ROS scavenging activity of the test sample was measured by the conversion of cupric (Cu^{2+})–ligand into cuprous (Cu^{+})–ligand by the anti-oxidant. Commonly, neocuproine, which is a chelating agent, acts as a ligand.[53] We also evaluated the CUPRAC of the LED-mediated green-synthesized AgNPs and found that B-DS-AgNPs had the highest antioxidant capacity, which was measured to be 588.1 ± 8.4 μM TEAC. This is because the blue LED helped in fine-tuning the size and shape of the AgNPs during their synthesis, which consequently also increased their antioxidant potential compared to the other AgNPs. R-DS-AgNPs also displayed good cupric reducing capacity of 546.6 ± 14 μM TEAC, while W-DS-AgNPs showed

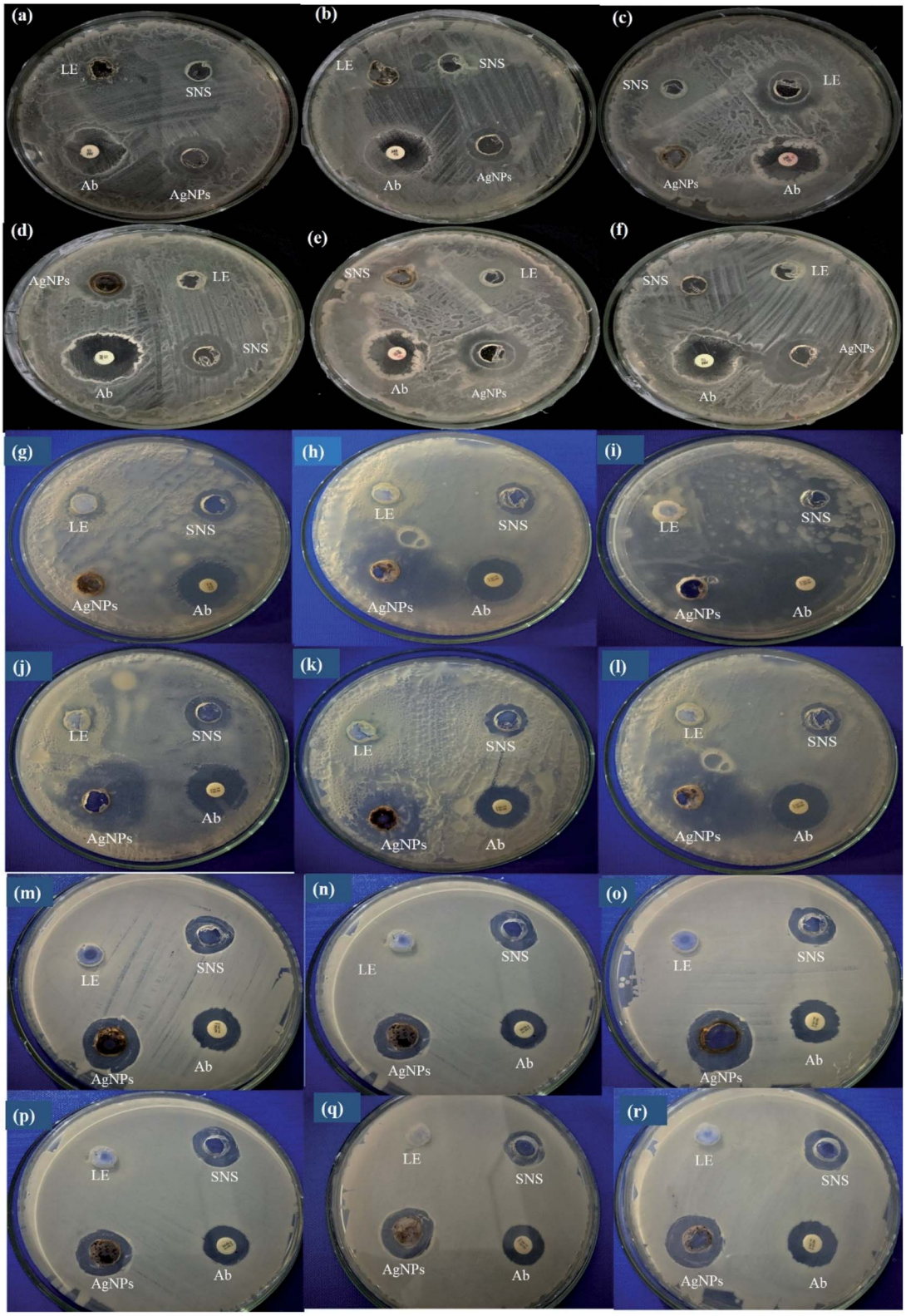

Fig. 8 Antibacterial activity of AgNPs against *B. subtilis*. (a) DS-AgNPs, (b) G-DS-AgNPs, (c) W-DS-AgNPs, (d) B-DS-AgNPs, (e) Y-DS-AgNPs and (f) R-DS-AgNPs. Against *P. aeruginosa* (g) DS-AgNPs, (h) G-DS-AgNPs, (i) W-DS-AgNPs, (j) B-DS-AgNPs, (k) Y-DS-AgNPs and (l) R-DS-AgNPs. Against *P. fluorescens* (m) DS-AgNPs, (n) G-DS-AgNPs, (o) W-DS-AgNPs, (p) B-DS-AgNPs, (q) Y-DS-AgNPs and (r) R-DS-AgNPs.

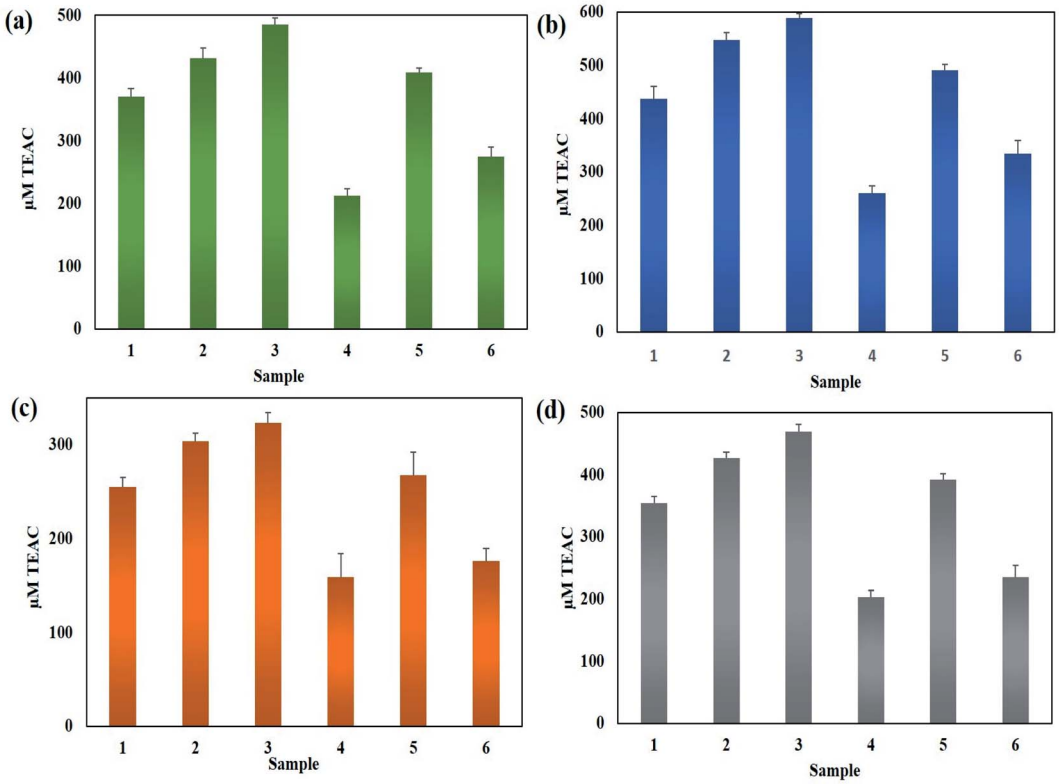

Fig. 9 Antioxidant assays of AgNPs. (a) FRAP, (b) CUPRAC, (c) ABTS and (d) ORAC (note- 1: DS-AgNPs; 2: R-DS-AgNPs; 3: B-DS-AgNPs; 4: Y-DS-AgNPs; 5: W-DS-AgNPs; and 6: G-DS-AgNPs).

a moderate value of 490.9 ± 11.4 µM TEAC, followed by G-DS-AgNPs of 334.6 ± 24.4 µM TEAC and the lowest by Y-DS-AgNPs of 259.3 ± 14.9 µM TEAC (Fig. 9b). This trend is consistent with the results of the FRAP assay. Studies on the evaluation of AgNP antioxidant potential using the CUPRAC method are scarce but N. Muniyappan and N. S. Nagarajan[54] reported the considerable antioxidant potential of AgNPs compared to plant extract measured by CUPRAC.

3.5.3 ABTS assay. ABTS is a free radical used to measure the relative ability of antioxidants to scavenge the ABTS generated in the aqueous phase.[55] The ABTS cation scavenging activity of B-DS-AgNPs was found to be the highest at 323.4 ± 10.4 µM TEAC compared to the control DS-AgNPs at 255 ± 10.5 µM TEAC (Fig. 9c). In contrast, Y-DS-AgNPs showed the least scavenging activity of 158.6 ± 25.1 µM TEAC. The other AgNPs also displayed considerable antioxidant activity including R-DS-AgNPs of 303.8 ± 8.2 µM TEAC, W-DS-AgNPs of 267.8 ± 24.2 µM TEAC and G-DS-AgNPs of 175.8 ± 13.2 µM TEAC. Moteriya *et al.*[56] also demonstrated the antioxidant potential of AgNPs measured *via* the ABTS method to be between 27–73%, showing their ability to treat stress-related disorders. Moreover, Baskaran *et al.*[57] also demonstrated the excellent antioxidant potential of biogenic AgNPs in terms of ABTS scavenging activity, which was found to be 8592.70 $\mu mol_{Trolox}\, g^{-1}$ compared to the control. These results show the outstanding potential of green AgNPs, particularly B-DS-AgNPs, as antioxidants, which is the mechanism by which NPs mediate their therapeutic activity.

3.5.4 ORAC assay. The oxygen radical absorbance capacity method evaluates the antioxidant potential of AgNPs by measuring their scavenging activity against peroxyl radicals, which are formed as a result of the decomposition of 2,2-azobis(2-methylpropionamidine) dihydrochloride.[50] We also measured the capacity of AgNPs to absorb oxygen radicals, where B-DS-AgNPs again showed significant activity of 469.2 ± 11.3 µM TEAC. For R-DS-AgNPs, their ORAC was found to be 426.7 ± 9.7 µM TEAC, W-DS-AgNPs 392.1 ± 9.4 µM TEAC, and G-DS-AgNPs 234.8 ± 19.3 µM TEAC, while Y-DS-AgNPs showed the least activity of 202.6 ± 11.4 µM TEAC, with the control DS-AgNPs showing 354.9 ± 9.7 µM TEAC (Fig. 9d). Our results are consistent with the previous study where AgNPs (5.2 nm) synthesized using *Solanum mammosum* leaf extract displayed significant ORAC activity of 637.5 ± 14.8 $\mu M_{ET}\, g^{-1}$.[58] Given that oxidative stress is associated with progressive cell damage and death, the significant ORAC activity of the LED-mediated green-synthesized AgNPs, particularly B-DS-AgNPs, shows their potential use in the treatment of degenerative and autoimmune disorders.[59] Overall, Y-DS-AgNPs and R-DS-AgNPs showed the lowest antioxidant activities, which can be attributed to their triangular shape in comparison to the spherical shape of W, G and B-DS-AgNPs. The shape-dependent catalytic and biological activity can be explained by the fact that different shapes tend to proliferate certain crystal facets, and these facets have varying activities.[60] Many previous studies also supported our results, where triangular-shaped AgNPs showed the least antioxidant activity compared to spherical- and rod-shaped AgNPs.[55,61]

3.6. Anti-glycation activities of LED-mediated green-synthesized AgNPs

Advanced glycation end-products are formed and accumulated at an accelerated rate during conditions such as diabetes mellitus, neurological diseases, cardiovascular diseases and aging processes.[62–64] Studies on the potential of AgNPs as anti-glycation agents have been carried out with positive results.[19] In this study, we also measured the anti-glycation activity of AgNPs in terms of % inhibition of pentosidine-like AGEs and vesperlysine-like AGEs. Interestingly, B-DS-AgNPs displayed the highest anti-glycation activity of 33.1% ± 3% and 63.3% ± 2% inhibition of pentosidine-like AGEs and vesperlysine-like AGEs, respectively. R-DS-AgNPs inhibited 30.4% ± 2.2% and 61.7% ± 1.8%, while W-DS-AgNPs inhibited 25.5% ± 3.1% and 52.8% ± 2.1% of pentosidine-like AGEs and vesperlysine-like AGEs, respectively. In contrast, G-DS-AgNPs and Y-DS-AgNPs showed the lowest level of anti-glycation activity (Fig. 10a and b), respectively.

Recently, Jan *et al.*[65] reported the significant inhibition of vesperlysine-like AGEs (up to 31.36% ± 1.19%) and pentosidine-like AGEs (up to 34.40% ± 1.16%). Compared to ZnONPs, AgNPs showed better ability to inhibit the formation of AGEs, as reported with up to 44.63% ± 1.26% and 37.13% ± 1.99% inhibition of pentosidine- and vesperlysine-like AGEs by ZnONPs, respectively.[66] Previous reports suggest that NPs interact with biomolecules differently, which is attributed to factors such as the size of NPs.[67] This fact has been reinforced by our findings that the smaller-sized and non-spherical B-DS-AgNPs inhibited the formation of AGEs the most. These results shows the potential of DS-AgNPs as anti-diabetic and anti-aging agents.

3.7. Anti-cancer activities of AgNPs

3.7.1 Measurement of cell viability of HepG2 cells. The use of plant-based AgNPs is a new approach to treat cancer due to their unique features. Thus, to assess the anti-cancer potential of the AgNPs, the antiproliferative activity of the LED-mediated green-synthesized AgNPs was measured by the MTT assay in terms of cell viability (Fig. 11a). We found the lowest viability of 26.01% ± 1.56% of HepG2 cells when exposed to Y-DS-AgNPs, which can be attributed to their triangular morphology having higher penetrative ability. Furthermore, smaller-sized NPs have direct contact with the cell surface and initiates cytotoxicity.[68] In contrast, the spherical-shaped W-DS-AgNPs and G-DS-AgNPs resulted in reduced cell viability of 43.19% ± 3.01% and 39.95% ± 3.05%, respectively. The shape of NPs has been reported to influence their cytotoxicity, where spherical AgNPs were less cytotoxic towards A549 cells compared to nano-wires, which induced negative outcomes.[69] B-DS-AgNPs also resulted in significantly low cell viability of 32.09% ± 1.33%, which is due to their smaller size. Lastly, R-DS-AgNPs resulted in 38.19% ± 2.92% viability, while the NTC cells were 100% viable. The good anti-cancer activity of R-DS-AgNPs can be attributed to their triangular shape. The shape-dependent catalytic and biological activity can be explained by the fact that different shapes tend to proliferate certain crystal facets, and these facets have varying activities.[60,70] These results reinforce the fact that the successful application of AgNPs depends on their physico-chemical properties, which are enhanced by LED exposure during their synthesis.

3.7.2 Measurement of intracellular ROS/RNS. The primary mechanism of AgNPs in killing cancer cells is through the formation of ROS, which results in a reduction in antioxidant potential. The resulting increase in intracellular ROS/RNS stimulates cancer cell death through harmful functions of ROS or *via* the apoptosis signalling pathway.[71] Y-DS-AgNPs resulted in ROS production (3807.62 ± 236.63 relative DHR-123 fluorescence unit (RFU DHR-123), which is consistent with the low cell viability. B-DS-AgNPs also resulted in significant ROS production of 3082.54 ± 130.76 RFU DHR-123. Furthermore, R-DS-AgNPs showed a value of 2596.54 ± 191.90 RFU DHR-123, W-DS-AgNPs 2295.01 ± 156.47 RFU DHR-123 and G-DS-AgNPs showed 2482.18 ± 183.13 RFU DHR-123 ROS production. Given that the NTC were viable, their ROS/RNS

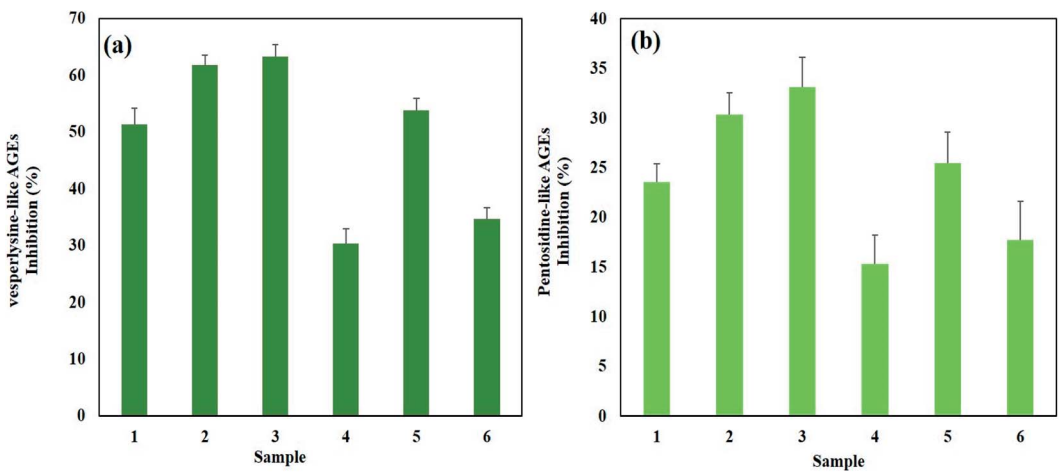

Fig. 10 Antiglycation activities of AgNPs. (a) Inhibition of vesperlysine-like AGEs and (b) pentosidine-like AGEs (note 1: DS-AgNPs; 2: R-DS-AgNPs; 3: B-DS-AgNPs; 4: Y-DS-AgNPs; 5: W-DS-AgNPs; and 6: G-DS-AgNPs).

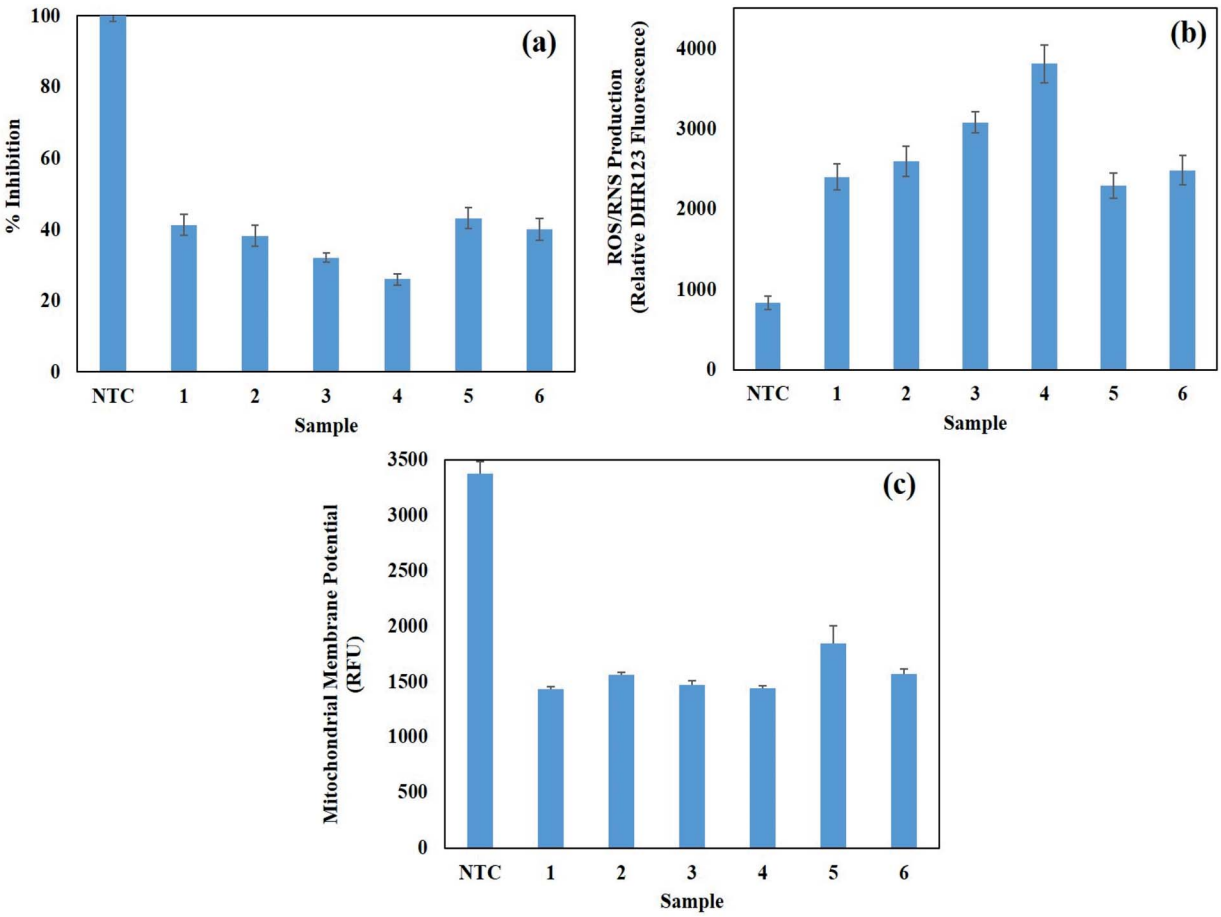

Fig. 11 Anti-cancer activities of AgNPs against HepG2 cells (a) % cell viability, (b) ROS/RNS production and (c) mitochondrial membrane potential in response to AgNP treatment (note 1: DS-AgNPs; 2: R-DS-AgNPs; 3: B-DS-AgNPs; 4: Y-DS-AgNPs; 5: W-DS-AgNPs; and 6: G-DS-AgNPs).

production level was as low as 835.00 ± 80.17 RFU DHR-123, while DS-AgNPs resulted in moderate ROS production of 2400.42 ± 163.93 RFU DHR-123 (Fig. 11b). Chuy *et al.*[72] also reported an increase in ROS production in the L929 cell line compared to normal cells when treated with green nano-architectonics of AgNPs. An increase in ROS/RNS production was observed with a decrease in AgNP size, which suggests that LEDs are effective in controlling the morphology of AgNPs, which in turn enhances their anti-cancer efficacy.

3.7.3 Mitochondrial membrane potential measurement. Oxidative stress results in a loss of MMP, which can be evaluated using rhodamine 123 dye. This dye is cell membrane permeable and localizes in the mitochondria of viable cells; however, when the MMP of the cell is disrupted, Rh123 is released and the intensity of its fluorescence decreases.[73] DS-AgNPs resulted in 1435.19 ± 19.31 RFU loss in MMP, while Y-DS-AgNPs led to 1440.87 ± 22.15 RFU. B-DS-AgNPs decreased the fluorescence to 1473.20 ± 36.60 RFU, G-DS-AgNPs to 1571.69 ± 43.93 RFU, R-DS-AgNPs to 1564.63 ± 17.39 RFU and W-DS-AgNPs to 1839.29 ± 162.45 RFU (Fig. 11c). AgNPs triggers cytotoxicity by targeting mitochondria and damaging their structure and morphology, resulting in the loss of mitochondrial function.[74] AgNPs cause a notable loss of MMP in various cell lines including ovarian cancer cells.[75] In accordance with our findings, Yuan *et al.*[76] found a significant disruption of MMP in HeLa cells in response to 1 μM AgNPs, while a further loss of MMP was observed when treated with a combination of AgNPs and the anticancer drug camptothecin. These findings show the ability of green-synthesized AgNPs especially the smaller-sized Y-DS-AgNPs and B-DS-AgNPs to disrupt the mitochondrial membrane potential as a way to treat cancer.

3.7.4 Caspase-3 gene expression and caspase-3/7 activity. The activation of the caspase cascade *via* the intrinsic mitochondrial pathway involves caspases 3 and 7, which are executioner caspases.[77] Fig. 12a shows the level of caspase-3 gene expression in HepG2 cells when exposed to the AgNPs. Significantly, Y-DS-AgNPs led to the highest caspase-3 gene expression (419.15% ± 106.51% in log 2-fold change compared to the control NTC). B-DS-AgNPs resulted in 243.70% ± 28.80%, G-DS-AgNPs 239.07% ± 11.40%, W-DS-AgNPs 179.12% ± 24.00% and R-DS-AgNPs 157.92% ± 14.53%. The control DS-AgNPs led to 154.20% ± 12.66% caspase-3 gene expression, while NTC showed 100% ± 1.81%. Similarly, a higher level of caspase-3/7 activity was observed in HepG2 cells when treated with AgNPs compared to NTC (normalized to 100 ± 6.61 RFU per mg protein), as shown in Fig. 12b. The control DS-AgNPs resulted in

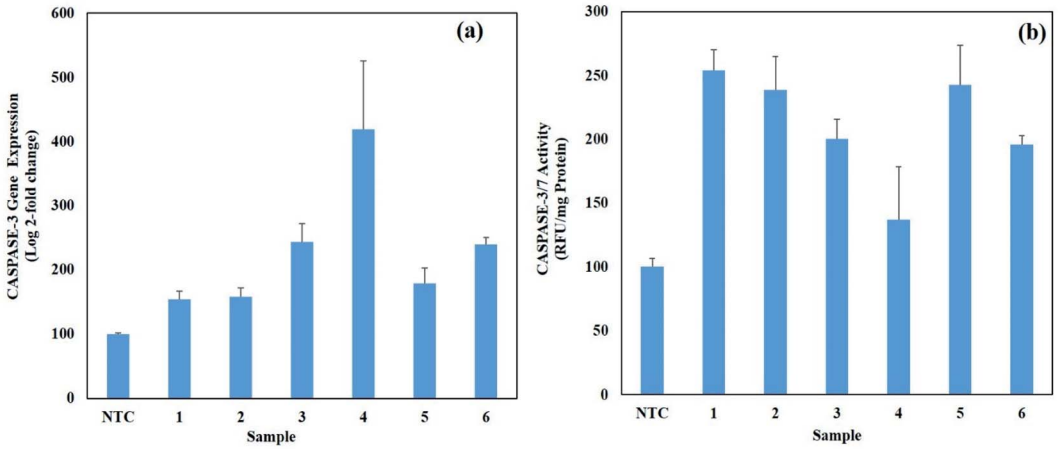

Fig. 12 (a) Caspase 3 gene expression and (b) caspase 3/7 activity of HepG2 cells when treated with AgNPs (note 1: DS-AgNPs; 2: R-DS-AgNPs; 3: B-DS-AgNPs; 4: Y-DS-AgNPs; 5: W-DS-AgNPs; and 6: G-DS-AgNPs).

253.79 ± 16.12, R-DS-AgNPs 238.62 ± 26.52, B-DS-AgNPs 200.43 ± 15.22, Y-DS-AgNPs 137.26 ± 41.13, W-DS-AgNPs 242.43 ± 30.81 and G-DS-AgNPs 195.72 ± 7.17 RFU per mg protein level of caspase-3/7 activity. Previous findings also showed an increase in caspase-3 gene expression and caspase-3/7 activity in response to *Morus macroura*-mediated AgNPs synthesized under high-energy UV-C light.[78] The increase in the level of effector caspase-3 activity was two-fold higher in MCF-7 breast cancer cells when treated with spherical-shaped green-synthesized AgNPs (10–60 nm) compared to the control.[79] AgNPs mediate cytotoxicity by effectively activating the caspase cascade and induce apoptosis in various cancer cells.[80] We also found the extraordinary potential of AgNPs particularly Y-DS-AgNPs in inducing caspase-3 gene expression and capsase-3/7 activities.

3.7.5 Postulated mechanism of anti-cancer activity of AgNPs. Nanoparticles hold potential to treat and diagnose cancer given that existing cancer treatments are associated with several challenges such as drug resistance by cancer, localization of anti-cancerous therapy at tumor sites and short drug circulation time.[81] NPs play an important role in programmed cell death by regulating the expression of proteins such as Bcl_2, P53 and caspases, which leads to intrinsic or extrinsic pathway activation. Activation of these proteins result in DNA fragmentation, cell blebbing and cell death.[82]

In the extrinsic pathway, apoptosis is initiated through the interaction of ligands and death receptors such as tumor receptors and the Fas receptor on the cell surface.[83] These receptors have death domains called the Fas-associated death domain (FADD) protein, which possess various upstream inactive procaspases (caspase 8 and 10). When these caspases are activated, they activate the death signaling complex and other caspases (3, 6 and 7). Here, notably caspase 8 caused cell death by the direct or indirect method. In the direct method, caspase 3 and caspase 7 are activated, whereas in the indirect method, BH3 proteins are activated, which convert BID proteins into tBID. Here, the extrinsic cycle and indirect process are linked.[84]

The intrinsic pathway starts as a result of the induction of cellular and oxidative stress by stimuli such as nanoparticles. In response to these stresses and tBID from the extrinsic pathway, the mitochondrial membrane ruptures, which initiates the caspases cascade. Mitochondria play an important role in the intrinsic pathway given that mitochondrial pore opening leads to the depolarization of the mitochondrial membrane. The rupture of mitochondria leads to cytochrome c discharge in the cytosol, which activates $APAF_1$ and permeabilizes the mitochondrial outer membrane. This leads to the discharge of Bcl_2 and soluble proteins to form apoptosomes.[85] The formation of apoptosomes marks the activation of caspase-9, followed by the activation of effector caspase-3. Consequently, DNA fragmentation, cell blebbing and apoptosis occurs in cells.[86] The proposed mechanism is summarized in Fig. 13.

3.8. Biocompatibility of AgNPs

3.8.1 Brine shrimp lethality assay. The brine shrimp lethality assay is an economical and simple way to assess the toxicological effects of NPs on living organisms.[87] In this study, the toxicity of green-synthesized LED-mediated AgNPs was evaluated against *Artemia salina* in terms of LC_{50}, where values between 10.0–30.0 μg mL^{-1} are considered as moderate toxicity.[21] A well-known chemotherapeutic agent, doxorubicin, was used as a positive control, presenting an LC_{50} value of 5.92 μg mL^{-1}, which is considered a highly toxic compound. In our study, AgNPs were found to be moderately toxic, where the LC_{50} for control DS-AgNPs was reported to be 21.32 ± 0.47 μg mL^{-1}. The other AgNPs also showed moderate toxicity, where R-DS-AgNPs (23.32 ± 1.06), B-DS-AgNPs (24.78 ± 0.22), Y-DS-AgNPs (27.94 ± 0.69), W-DS-AgNPs (23.80 ± 0.67) and G-DS-AgNPs (26.81 ± 0.24), as depicted in Fig. 14a. Similarly, Singh *et al.*[88] found that AgNPs synthesized using the extract of *Ipomoea carnea* were non-toxic towards brine shrimps; however, their toxicity increased in a concentration-dependent manner. Given that the toxicity of the smaller-sized Y-DS-AgNPs tended more towards mild toxicity, they can be used as commercial anti-cancerous agents given that they were the most cytotoxic, while being safe on the environment and living organisms. The

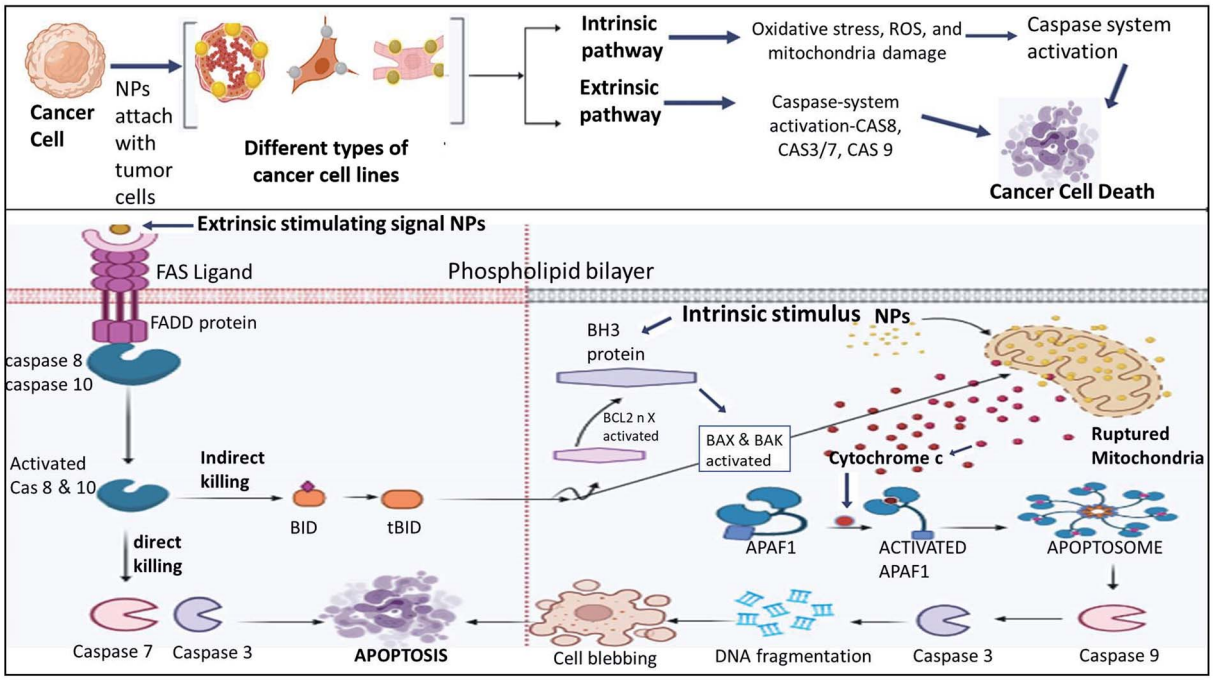

Fig. 13 Proposed mechanism of anti-cancer activity of AgNPs.

moderately toxic nature of AgNPs can be further reduced under different conditions given that the experimental and environmental conditions influence the results of aquatic nanotoxicity.[89]

3.8.2 Biocompatibility with human red blood cells (hRBCs). The compatibility of AgNPs was evaluated with hRBCs to determine their biosafe nature. All the AgNPs were found to be mildly hemolytic given that they hemolysed hRBCs between 2–5% according to the standards of the American Society for Testing and Materials Designation.[90] The control DS-AgNPs resulted in 3.58% ± 0.24% hemolysis, while that by W-DS-AgNPs was 3.42% ± 0.23%, G-DS-AgNPs was 3.70% ± 0.27% and R-DS-AgNPs was 3.87% ± 0.29%. However, B-DS-AgNPs resulted in the highest hemolysis level of 4.59% ± 0.19% and Y-DS-AgNPs 4.67% ± 0.35% (Fig. 14b). Here, it can be deduced that the green-synthesized AgNPs exhibit biocompatibility for human use as an alternate drug given that 5% hemolysis is acceptable for biomaterials.[91] Y-DS-AgNPs and B-DS-AgNPs showed the greatest hemolytic nature, which can be due to their smaller size, where factors such as higher concentration, smaller size and longer exposure time of NPs can cause hemolysis and morphological changes in RBCs.[92] Kumar *et al.*[93] reported the high hemo-compatibility of surface-modified gold NPs, while our AgNPs showed similar compatibility without any surface modification. Also, the biocompatibility of AgNPs could be further enhanced by reducing the concentration of AgNPs.

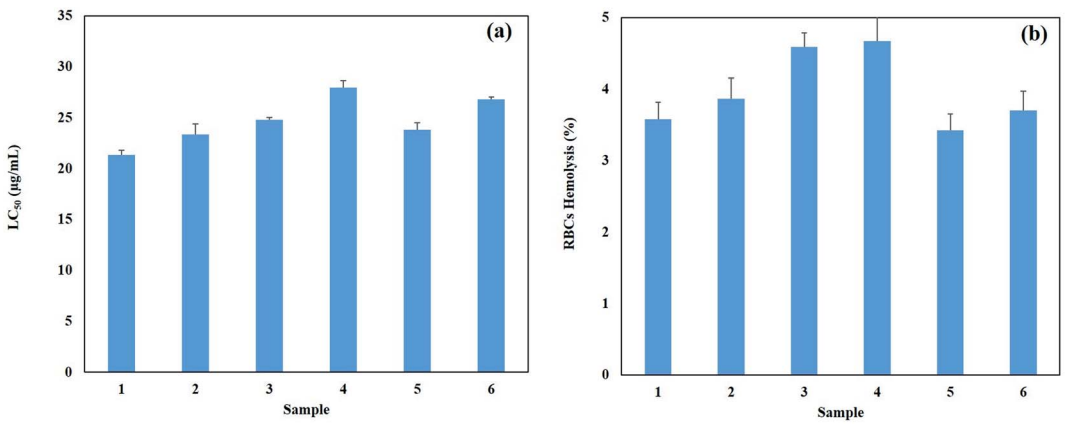

Fig. 14 Biocompatibility studies of green-synthesized AgNPs. (a) Toxicity of AgNPs against brine shrimp. (b) Biocompatibility of AgNPs with human red blood cells (hRBCs). (Note 1: DS-AgNPs; 2: R-DS-AgNPs; 3: B-DS-AgNPs; 4: Y-DS-AgNPs; 5: W-DS-AgNPs; and 6: G-DS-AgNPs).

4. Conclusions

AgNPs are one of the most commonly synthesized, investigated, and utilized representatives of nanomaterials due to their excellent optical, catalytical, and biological properties. AgNPs are well-known for their broad-spectrum and highly efficient antimicrobial and anticancer activities. Other biological activities of AgNPs have been also explored, including promoting bone healing and wound repair, enhancing the immunogenicity of vaccines, anti-diabetic and anti-aging effects. Due to the numerous biological and clinical applications of AgNPs, in this study, they were bio-synthesized from *D. sissoo* leaf extract under LED exposure. The phytochemical analysis of *D. sissoo* showed that the plant extract was rich in flavonoid and phenolic content, and thereby resulted in increased free radical scavenging activity. The FTIR analysis revealed that biologically active plant ingredients including alcohols and phenolic compounds acted as bio-reductants and stabilizers of AgNPs. Further characterization by SEM-EDX showed that the LEDs promoted the synthesis of uniquely shaped AgNPs together with increased elemental percentage of Ag in AgNPs compared to the control AgNPs. A decrease in size and well defined shape were observed in the case of the yellow and blue LED-mediated green synthesis of AgNPs. Given that the morphology of NPs determine their applications and influence their efficacy, in our study, B-DS-AgNPs showed unusually high anti-oxidant activities, as reflected by the inhibition of AGE formation and best anti-bacterial activity by B-DS-AgNPs. Alternatively, the smaller-sized Y-DS-AgNPs showed exceptionally good anticancer activities, where HepG2 cells showed the least viability due to the highest intracellular ROS/RNS production and distribution of MMP by Y-DS-AgNPs. Furthermore, all the AgNPs showed mild hemolysis towards hRBCs and moderate toxicity against brine shrimp, which could be further improved by using a lower concentration of AgNPs. Our research showed the promising role of LEDs in modifying the physico-chemical characteristics of AgNPs during the synthesis, which was consequently reflected in their effective biological activities. Studying and optimizing other factors such as incubation time, concentration of plant extract, temperature, and pH can further improve the quality and yield of AgNPs. Also, concentration-dependent biological studies should be carried out to further enhance their efficacy. When the synthesis of AgNPs is optimized and upscaled to an industrial level, these biocompatible AgNPs can be used for therapeutic applications.

Conflicts of interest

The authors declare that they have no conflict of interest.

References

1 A. K. Khan, S. Renouard, S. Drouet, J.-P. Blondeau, I. Anjum, C. Hano, B. H. Abbasi and S. Anjum, *Pharmaceutics*, 2021, **13**, 1977.
2 C. Singh, R. Baboota and P. Naik, *Adv. Mater. Lett.*, 2012, **3**, 279–285.
3 K. G. Stamplecoskie and J. C. Scaiano, *J. Am. Chem. Soc.*, 2010, **132**, 1825–1827.
4 J.-H. Lee, P. Velmurugan, J.-H. Park, K. Murugan, N. Lovanh, Y.-J. Park, B.-T. Oh, P. Venkatachalam and G. Benelli, *Physiol. Mol. Plant Pathol.*, 2018, **101**, 178–186.
5 B. Kumar, Y. Angulo, K. Smita, L. Cumbal and A. Debut, *Particuology*, 2016, **24**, 123–128.
6 P. Thuesombat, S. Hannongbua, S. Akasit and S. Chadchawan, *Ecotoxicol. Environ. Saf.*, 2014, **104**, 302–309.
7 I. X. Yin, J. Zhang, I. S. Zhao, M. L. Mei, Q. Li and C. H. Chu, *Int. J. Nanomed.*, 2020, **15**, 2555.
8 M. Wypij, T. Jędrzejewski, J. Trzcińska-Wencel, M. Ostrowski, M. Rai and P. Golińska, *Front. Microb.*, 2021, **12**, 632505–632522.
9 J. M. Ashraf, M. A. Ansari, H. M. Khan, M. A. Alzohairy and I. Choi, *Sci. Rep.*, 2016, **6**, 20414.
10 R. L. Prior, X. Wu and K. Schaich, *J. Agric. Food Chem.*, 2005, **53**, 4290–4302.
11 S. Anjum, B. H. Abbasi and C. Hano, *Plant Cell, Tissue Organ Cult.*, 2017, **129**, 73–87.
12 S. Anjum and B. H. Abbasi, *Int. J. Nanomed.*, 2016, **11**, 715.
13 D. Tungmunnithum, S. Renouard, S. Drouet, J.-P. Blondeau and C. Hano, *Plants*, 2020, **9**, 921.
14 S. Fakhari, M. Jamzad and H. Kabiri Fard, *Green Chem. Lett. Rev.*, 2019, **12**, 19–24.
15 B. H. Abbasi, S. Anjum and C. Hano, *RSC Adv.*, 2017, **7**, 15931–15943.
16 B. H. Abbasi, A. Siddiquah, D. Tungmunnithum, S. Bose, M. Younas, L. Garros, S. Drouet, N. Giglioli-Guivarc'h and C. Hano, *Int. J. Mol. Sci.*, 2019, **20**, 452.
17 Ş. Karaman, E. Tütem, K. Sözgen Başkan and R. Apak, *Food Chem.*, 2010, **120**, 1201–1209.
18 K. Thaipong, U. Boonprakob, K. Crosby, L. Cisneros-Zevallos and D. H. Byrne, *J. Food Compos. Anal.*, 2006, **19**, 669–675.
19 M. Shah, S. Nawaz, H. Jan, N. Uddin, A. Ali, S. Anjum, N. Giglioli-Guivarc'h, C. Hano and B. H. Abbasi, *Mater. Sci. Eng., C*, 2020, **112**, 110889.
20 M. Nazir, D. Tungmunnithum, S. Bose, S. Drouet, L. Garros, N. Giglioli-Guivarc'h, B. H. Abbasi and C. Hano, *J. Agric. Food Chem.*, 2019, **67**, 1847–1859.
21 M. Ahmed, H. Fatima, M. Qasim and B. Gul, *BMC Complementary Altern. Med.*, 2017, **17**, 1–16.
22 A. T. Khalil, M. Ovais, I. Ullah, M. Ali, Z. K. Shinwari, S. Khamlich and M. Maaza, *Nanomedicine*, 2017, **12**, 1767–1789.
23 R. Kamboj, M. B. Bera and V. Nanda, *Int. J. Food Sci. Technol.*, 2013, **48**, 578–587.
24 S. Yasmeen and P. Gupta, *J. Herb. Med.*, 2021, **29**, 100456.
25 G. Marslin, K. Siram, Q. Maqbool, R. K. Selvakesavan, D. Kruszka, P. Kachlicki and G. Franklin, *Materials*, 2018, **11**, 940.
26 E. Vadivel, R. D. Tendulkar and V. V. Harmalkar, *Int. J. Curr. Pharm. Res.*, 2015, **7**, 70–72.
27 J. Jalab, W. Abdelwahed, A. Kitaz and R. Al-Kayali, *Heliyon*, 2021, **7**, e08033.
28 T. D. Nguyen, D. P. Nguyen, Y. H. Hoang, T. T. Nguyen and H. T. Nguyen, *Chem. Pap.*, 2021, **75**, 5623–5631.

29 K. Anandalakshmi, J. Venugobal and V. Ramasamy, *Appl. Nanosci.*, 2016, **6**, 399–408.
30 O. Maitera and I. Chukkol, *World J. Adv. Res. Rev.*, 2016, **3**, 25–29.
31 I. Ali, G. Rizwani, H. Shareef and S. Khan, *Int. J. Pharm. Pharm. Sci.*, 2016, **8**, 48–53.
32 S. Bawazeer, A. Rauf, S. U. A. Shah, A. M. Shawky, Y. S. Al-Awthan, O. S. Bahattab, G. Uddin, J. Sabir and M. A. El-Esawi, *Green Process. Synth.*, 2021, **10**, 85–94.
33 T. Varadavenkatesan, R. Selvaraj and R. Vinayagam, *Mater. Today: Proc.*, 2019, **23**, 39–42.
34 P. Jegadeeswaran, R. Shivaraj and R. Venckatesh, *Digest Journal of Nanomaterials and Biostructures*, 2012, **7**, 991–998.
35 J. Saha, A. Begum, A. Mukherjee and S. Kumar, *Sustainable Environ. Res.*, 2017, **27**, 245–250.
36 A. Rautela, J. Rani and M. Debnath, *J. Anal. Sci. Technol.*, 2019, **10**, 5–15.
37 A. M. Soliman, W. Abdel-Latif, I. H. Shehata, A. Fouda, A. M. Abdo and Y. M. Ahmed, *Biol. Trace Elem. Res.*, 2021, **199**, 800–811.
38 A. C. Reboli and W. E. Farrar, in *Laboratory Diagnosis of Infectious Diseases*, Springer, 1988, pp. 69–82.
39 F. Arancibia, T. T. Bauer, S. Ewig, J. Mensa, J. Gonzalez, M. S. Niederman and A. Torres, *Arch. Intern. Med.*, 2002, **162**, 1849–1858.
40 T. Nishimura, K. Hattori, A. Inoue, T. Ishii, T. Yumoto, K. Tsukahara, A. Nakao, S. Ishihara and S. Nakayama, *World J. Emerg. Med.*, 2017, **8**, 151.
41 R. Balachandar, R. Navaneethan, M. Biruntha, K. K. A. Kumar, M. Govarthanan and N. Karmegam, *Mater. Lett.*, 2022, **311**, 131572.
42 A. K. Keshari, R. Srivastava, P. Singh, V. B. Yadav and G. Nath, *J. Ayurveda Integr. Med.*, 2020, **11**, 37–44.
43 G.-A. Martínez-Castañon, N. Nino-Martinez, F. Martinez-Gutierrez, J. Martinez-Mendoza and F. Ruiz, *J. Nanopart. Res.*, 2008, **10**, 1343–1348.
44 J. Li, K. Rong, H. Zhao, F. Li, Z. Lu and R. Chen, *J. Nanosci. Nanotechnol.*, 2013, **13**, 6806–6813.
45 T. Dutta, S. K. Chowdhury, N. N. Ghosh, A. P. Chattopadhyay, M. Das and V. Mandal, *J. Mol. Struct.*, 2022, **1247**, 131361.
46 X. Yan, B. He, L. Liu, G. Qu, J. Shi, L. Hu and G. Jiang, *Metallomics*, 2018, **10**, 557–564.
47 H. Kumar, L. Franzetti, A. Kaushal and D. Kumar, *Ann. Microbiol.*, 2019, **69**, 873–883.
48 S. CG Kiruba Daniel, K. Nehru and M. Sivakumar, *Curr. Nanosci.*, 2012, **8**, 125–129.
49 A. Danet, in *Antioxidants - Benefits, Sources, Mechanisms of Action*, ed. V. Waisundara, IntechOpen, 2021, DOI: **10.5772/intechopen.96654**.
50 E. Mfotie Njoya, in *Cancer*, ed. V. R. Preedy and V. B. Patel, Academic Press, San Diego, 2nd edn, 2021, pp. 349–357, DOI: **10.1016/B978-0-12-819547-5.00031-6**.
51 Y. Zhong and F. Shahidi, in *Handbook of Antioxidants for Food Preservation*, ed. F. Shahidi, Woodhead Publishing, 2015, pp. 287–333, DOI: **10.1016/B978-1-78242-089-7.00012-9**.
52 A. Balciunaitiene, P. Viskelis, J. Viskelis, P. Streimikyte, M. Liaudanskas, E. Bartkiene, P. Zavistanaviciute, E. Zokaityte, V. Starkute and M. Ruzauskas, *Processes*, 2021, **9**, 1304.
53 M. Özyürek, K. Güçlü, E. Tütem, K. Sözgen Başkan, E. Erçağ, S. Karademir Çelik, S. Baki, L. Yıldız, Ş. Karaman and R. Apak, *Anal. Methods*, 2011, **3**, 2439–2453.
54 N. Muniyappan and N. S. Nagarajan, *Process Biochem.*, 2014, **49**, 1054–1061.
55 Z. Bedlovičová, I. Strapáč, M. Baláž and A. Salayová, *Molecules*, 2020, **25**, 3191.
56 P. Moteriya, H. Padalia and S. Chanda, *J. Genet. Eng. Biotechnol.*, 2017, **15**, 505–513.
57 X. Baskaran, A. V. G. Vigila, T. Parimelazhagan, D. Muralidhara-Rao and S. Zhang, *Int. J. Nanomed.*, 2016, **11**, 5789.
58 F. Pilaquinga, J. Morey, L. Fernandez, P. Espinoza-Montero, M. Moncada-Basualto, J. Pozo-Martinez, C. Olea-Azar, R. Bosch, L. Meneses and A. Debut, *Int. J. Nanomed.*, 2021, **16**, 5879.
59 R. Jaffe and J. Mani, in *Polyphenols: Mechanisms of Action in Human Health and Disease*, ed. R. R. Watson, V. R. Preedy and S. Zibadi, Academic Press, 2nd edn, 2018, pp. 403–413, DOI: **10.1016/B978-0-12-813006-3.00029-5**.
60 P. Bélteky, A. Rónavári, D. Zakupszky, E. Boka, N. Igaz, B. Szerencsés, I. Pfeiffer, C. Vágvölgyi, M. Kiricsi and Z. Kónya, *Int. J. Nanomed.*, 2021, **16**, 3021.
61 H. Kumar, K. Bhardwaj, E. Nepovimova, K. Kuča, D. Singh Dhanjal, S. Bhardwaj, S. K. Bhatia, R. Verma and D. Kumar, *Nanomaterials*, 2020, **10**, 1334.
62 K. Jandeleit-Dahm and M. E. Cooper, *Curr. Pharm. Des.*, 2008, **14**, 979–986.
63 L.-F. Lue, D. G. Walker, S. Jacobson and M. Sabbagh, *Future Neurol.*, 2009, **4**, 167–177.
64 S. Morales, J. A. García-Salcedo and M. Muñoz-Torres, *Med. Clin.*, 2010, **136**, 298–302.
65 H. Jan, G. Zaman, H. Usman, R. Ansir, S. Drouet, N. Gigliolo-Guivarc'h, C. Hano and B. H. Abbasi, *J. Mater. Res. Technol.*, 2021, **15**, 950–968.
66 H. Jan, M. Shah, A. Andleeb, S. Faisal, A. Khattak, M. Rizwan, S. Drouet, C. Hano and B. H. Abbasi, *Oxid. Med. Cell. Longevity*, 2021, **2021**, 4786227.
67 S. Anandan, M. Mahadevamurthy, M. A. Ansari, M. A. Alzohairy, M. N. Alomary, S. Farha Siraj, S. Halugudde Nagaraja, M. Chikkamadaiah, L. Thimappa Ramachandrappa and H. K. Naguvanahalli Krishnappa, *Biomolecules*, 2019, **9**, 882.
68 A. R. Gliga, S. Skoglund, I. O. Wallinder, B. Fadeel and H. L. Karlsson, *Part. Fibre Toxicol.*, 2014, **11**, 1–17.
69 L. C. Stoehr, E. Gonzalez, A. Stampfl, E. Casals, A. Duschl, V. Puntes and G. J. Oostingh, *Part. Fibre Toxicol.*, 2011, **8**, 1–15.
70 S. Pal, Y. K. Tak and J. M. Song, *Appl. Environ. Microbiol.*, 2007, **73**, 1712–1720.
71 A. Kocyigit, E. M. Guler and M. Dikilitas, *Reactive Oxygen Species in Living Cells*, InterchOpen, London, 2018, pp. 21–45.

72 G. P. Chuy, P. C. L. Muraro, A. R. Viana, G. Pavoski, D. C. R. Espinosa, B. S. Vizzotto and W. L. da Silva, *J. Inorg. Organomet. Polym. Mater.*, 2021, **32**(4), 1213–1222.
73 E. Huerta-García, I. Zepeda-Quiroz, H. Sánchez-Barrera, Z. Colín-Val, E. Alfaro-Moreno, M. D. P. Ramos-Godinez and R. López-Marure, *Molecules*, 2018, **23**, 1955.
74 J. Li, B. Zhang, X. Chang, J. Gan, W. Li, S. Niu, L. Kong, T. Wu, T. Zhang, M. Tang and Y. Xue, *Environ. Pollut.*, 2020, **256**, 113430.
75 Y.-G. Yuan, Q.-L. Peng and S. Gurunathan, *Int. J. Nanomed.*, 2017, **12**, 6487.
76 Y.-G. Yuan, S. Zhang, J.-Y. Hwang and I.-K. Kong, *Oxid. Med. Cell. Longevity*, 2018, **2018**, 21.
77 M. D'Amelio, V. Cavallucci and F. Cecconi, *Cell Death Differ.*, 2010, **17**, 1104–1114.
78 S. Anjum, A. K. Khan, A. Qamar, N. Fatima, S. Drouet, S. Renouard, J. P. Blondeau, B. H. Abbasi and C. Hano, *Int. J. Mol. Sci.*, 2021, **22**, 11294.
79 I. Ullah, A. T. Khalil, M. Ali, J. Iqbal, W. Ali, S. Alarifi and Z. K. Shinwari, *Oxid. Med. Cell. Longevity*, 2020, **2020**, 14.
80 A. A. Al-Khedhairy and R. Wahab, *Metals*, 2022, **12**, 148.
81 P. V. Rao, D. Nallappan, K. Madhavi, S. Rahman, L. Jun Wei and S. H. Gan, *Oxid. Med. Cell. Longevity*, 2016, **2016**, 3685671.
82 S. B. Bratton, G. Walker, S. M. Srinivasula, X. M. Sun, M. Butterworth, E. S. Alnemri and G. M. Cohen, *EMBO J.*, 2001, **20**, 998–1009.
83 A. Sarkar, J. Das, P. Manna and P. C. Sil, *Toxicology*, 2011, **290**, 208–217.
84 B. Kang, L. A. Austin and M. A. El-Sayed, *ACS Nano*, 2014, **8**, 4883–4892.
85 S. W. Tait and D. R. Green, *Nat. Rev. Mol. Cell Biol.*, 2010, **11**, 621–632.
86 S. Yuan, X. Yu, M. Topf, S. J. Ludtke, X. Wang and C. W. Akey, *Structure*, 2010, **18**, 571–583.
87 H. E. A. Mohamed, S. Afridi, A. T. Khalil, D. Zia, Z. K. Shinwari, M. S. Dhlamini and M. Maaza, *J. Inorg. Organomet. Polym. Mater.*, 2020, **30**, 3241–3254.
88 R. Singh and Navneet, *Curr. Res. Green Sustainable Chem.*, 2021, **4**, 100152.
89 R. Asadi Dokht Lish, S. A. Johari, M. Sarkheil and I. J. Yu, *Environ. Pollut.*, 2019, **255**, 113358.
90 N. H. Kumar, M. Murali, A. Satish, S. B. Singh, H. Gowtham, H. Mahesh, T. Lakshmeesha, K. Amruthesh and S. Jagannath, *J. Cluster Sci.*, 2020, **31**, 523–534.
91 M. Zare, K. Namratha, M. Thakur and K. Byrappa, *Mater. Res. Bull.*, 2019, **109**, 49–59.
92 T. Z. Mehrizi, *Nano*, 2021, **16**, 2130007.
93 S. Kumar, I. Jha, N. K. Mogha and P. Venkatesu, *Appl. Surf. Sci.*, 2020, **512**, 145573.